# Novel Pathogen Infections in the Clonal Raider Ant

A Thesis

submitted to

Indian Institute of Science Education and Research Pune in partial fulfillment of the requirements for the BS-MS Dual Degree Programme

by

Ashmita Baruah

20201235


Indian Institute of Science Education and Research Pune

Dr. Homi Bhabha Road, Pashan, Pune 411008, INDIA.

Date: March, 2025

Under the guidance of

Supervisor: Dr. Yuko Ulrich,

Max Planck Institute for Chemical Ecology

From May 2024 to March 2025

INDIAN INSTITUTE OF SCIENCE EDUCATION AND RESEARCH PUNE

# Certificate

This is to certify that this dissertation entitled “Novel Pathogen Infections in the Clonal Raider Ant” towards the partial fulfillment of the BS-MS dual degree programme at the Indian Institute of Science Education and Research, Pune represents study/work carried out by Ashmita Baruah at the Max Planck Institute for Chemical Ecology under the supervision of Dr. Yuko Ulrich, Group Leader, Lise Meitner Research Group, Social Behaviour, during the academic year 2024-2025.

(signature)

Dr. Yuko Ulrich

Group Leader

Lise Meitner Research Group

Max Planck Institute for Chemical Ecology

Committee:

Dr. Yuko Ulrich (Supervisor)

Dr. Sagar Pandit (Expert)

.

This thesis is dedicated to my mother,

Jyotirupa Thakur Baruah

# Declaration

I hereby declare that the matter embodied in the report entitled “ Novel Pathogen Infections in the Clonal Raider Ant ” are the results of the work carried out by me at the Department of Biology, Indian Institute of Science Education & Research (IISER) Pune, under the supervision of Dr. Yuko Ulrich, Group Leader, Lise Meitner Research Group, Social Behaviour, and the same has not been submitted elsewhere for any other degree. Wherever others contribute, every effort is made to indicate this clearly, with due reference to the literature and acknowledgment of collaborative research and discussions.

Ashmita Baruah

Roll no: 20201235

# Table of Contents

# List of Tables

# List of Figures

# Abstract

Social insects live in high-density colonies of genetically similar individuals making them susceptible to rapid pathogen transmission. While pathogens can have detrimental effects on host fitness, insect hosts employ various immune strategies in response to infection. Here we study host-pathogen interaction and transmission dynamics in the clonal raider ant, *Ooceraea biroi,* using the acute bee paralysis virus (ABPV) and *Sodalis praecaptivus.* We investigate the ability of these pathogens to replicate and transmit within host colonies and their impact on survival. To understand the host response, we investigate potential immune mechanisms. Our results indicate that ABPV does not infect or elicit an RNAi response in *O. biroi.* In contrast, *S. praecaptivus* successfully establishes infection across multiple life stages. *S. praecaptivus* localizes across the host body and impacts survival and fecundity. It also leads to changes in host melanization. However, neither pathogen exhibits transmission among colonymates. Together our findings contribute towards understanding infection dynamics in response to novel pathogens in *O. biroi.* These results also lay the groundwork for establishing a fluorescently tractable host-pathogen system in *O. biroi* that can be used for monitoring behaviour responses to infection progression within a colony.

# Acknowledgments

I would like to express my sincere gratitude to Dr. Yuko Ulrich for her support and guidance throughout my project. Her feedback and constructive criticism have contributed significantly to the development and refinement of this research. I am extremely grateful to Dr. Lai ka Lo who continuously guided me throughout the thesis. Her insights and mentorship have not only supported my research in the lab but also helped me develop as a researcher. I am also grateful to all the members of the lab, Sarah Rogoz, Tim Zetzsche, Sandra Tretter, Zimai Li, Dr. Irene Ng, and Dr. Baptist Piquere,t who constantly supported and shared their expertise with me throughout the project. I would like to especially thank Bhoomika Bhat, a senior PhD member of the lab who constantly encouraged me throughout the ups and downs of the project. I am incredibly grateful for the support I have received from all the technical assistants in the lab, Dr. Roland Spiess, Antje Schmaltz, and Wibke Seibt.

I am also thankful to Prof. Dr. Martin Kaltenpoth for his valuable support and collaboration on the *Sodalis* part of the project. I am grateful to the members of Insect Symbiosis Group for providing resources and guidance for various parts of the project: Ronja Kruesemer, who shared her valuable insights in working with the bacteria, and Dr. Benjamin Weiss, who supported me in the preparation of the FISH samples. I am also incredibly grateful to Dr. Viet Grabe, who shared his microscopy expertise with me and taught me the various methods of imaging.

I would also like to express my gratitude to Dr. Sagar Pandit, who shared his valuable advice as the expert on my project. I am grateful to IISER Pune for preparing me for this opportunity. I am thankful to the Max Planck Institute for Chemical Ecology for giving me this amazing opportunity to conduct my thesis research and for supporting my stay.

Finally, this thesis would not have been possible without the support of my family, who stood strong with me through all the challenging times. I am thankful to my amazing friends who supported, guided, motivated, and cheered me up throughout this scientific journey.

# Contributions

| Contributor name | Contributor role |
|---|---|
| Ashmita Baruah, Dr. Lai ka Lo, Dr. Yuko Ulrich | Conceptualization Ideas |
| Ashmita Baruah, Dr. Lai ka Lo, Dr. Benjamin Weiss | Methodology |
| - | Software |
| Ashmita Baruah | Validation |
| Ashmita Baruah | Formal analysis |
| Ashmita Baruah | Investigation |
| Dr. Yuko Ulrich, Prof. Dr. Martin Kaltenpoth | Resources |
| Ashmita Baruah | Data Curation |
| Ashmita Baruah | Writing - original draft preparation |
| Ashmita Baruah, Dr. Lai ka Lo, Dr. Yuko Ulrich | Writing - review and editing |
| Ashmita Baruah | Visualization |
| Dr. Yuko Ulrich, Dr. Lai ka lo | Supervision |
| Dr. Yuko Ulrich | Project administration |
| Dr. Yuko Ulrich | Funding acquisition |

# Chapter 1: Introduction

Group living offers several fitness advantages, including enhanced reproductive success, collective defense against predators, and improved foraging efficiency, enabling social insects like ants, termites, and some bees to colonize diverse habitats (Wilson, E.O 1971). Ants and termites alone constitute up to 55% of soil arthropod biomass, with the global ant population estimated at $20 \times 10^{15}$, equaling 20% of human biomass (Schultheiss et al. 2022; Rosenberg et al. 2023). However, the division of labor and task specialization within colonies necessitate frequent interactions that serve as potential routes for pathogen transmission (Sarkar et al. 2024). Social insects provide a high density of potential hosts that are genetically related (Schmid-Hempel 1995; Shykoff and Schmid-Hempel 1997). Additionally, vertical pathogen transmission through infected queens threatens colony survival (Schmid-Hempel 1998). This paradox of cooperative behaviors fostering both survival and vulnerability underscores the importance of understanding host-pathogen interactions in social insects.

Pathogens ranging from microorganisms like viruses, bacteria, fungi, and protozoans to macroscopic helminths like nematodes and trematodes are found in social insects (Schmid-Hempel 1998). These pathogens can impact host survival, physiology, and behavior and disrupt colony functions such as foraging, interaction networks etc. For example, honeybee viruses, such as deformed wing virus (DWV), black queen cell virus (BQCV), acute bee paralysis virus (ABPV), and Kashmir bee virus (KBV), can lead to a phenomenon known as Colony Collapse Disorder (CCD) (vanEngelsdorp et al. 2009; Tantillo et al. 2015). The parasitic fungus *Ophiocordyceps* hijacks the behavior of its host, the carpenter ant (*Camponotus* spp.), and forces the infected ant to distance itself from the colony, climb vegetation, and bite down onto leaves or twigs where the fungus kills the ant, sprouts a stalk, and releases infective spores (de Bekker and Das 2022). Other pathogens, like *Wolbachia* and *Sodalis*, exhibit more flexible associations, shifting between parasitism and mutualism depending on the host species and environmental conditions (Hosokawa et al. 2010; Clayton et al. 2012). Over evolutionary time, some pathogens may attenuate their virulence and transition into beneficial or neutral

symbionts, demonstrating the dynamic nature of these interactions (Ramdya et al. 2012).

To counter pathogen infections, social insects have evolved diverse immune strategies. Social insects display collective anti-parasite defenses called social immunity that allow avoidance, containment, or elimination of the parasite from the colony (Cremer et al., 2007; Meunier, 2015). Social immunity comprises multiple mechanisms, such as the application of antimicrobials on food and nesting materials and a range of hygiene behaviors to eliminate corpses and waste. In some ants and honeybees, infected individuals leave the nest to die, thus protecting the colony from further infection (Heinze and Walter 2010; Rueppell et al. 2010). Social insects actively groom each other to remove pathogens from the surface of the body, a phenomenon known as allogrooming. For example, fungus growing ants collect infectious material in pouches inside their mouths, which are sterilized using antimicrobials and ejected (Little et al. 2003). In addition, some social insects adjust their colony dynamics in response to the presence of pathogens. For instance, fungus-infected *Lasius niger* colonies alter their social networks to minimize disease transmission (Stroeymeyt et al. 2018). Honeybees (*Apis mellifera*) raise the temperature of their hive to inhibit the growth of pathogens, such as *Ascosphaera apis*, that cause chalkbrood disease (Starks et al. 2000). However, a large number of these studies use fungal pathogens (Starks et al. 2000; Westhus et al. 2014; Diez et al. 2015; Theis et al. 2015; Stroeymeyt et al. 2018) highlighting the importance of the development of new systems to explore immune interactions with a broader range of pathogens.

Despite the effectiveness of social immunity in limiting pathogen spread, individual immune responses remain crucial for defense against infections. Insects harbor humoral immune mechanisms like Jak/STAT (Janus kinase/Signal Transducer and Activator of Transcription), Toll, and Imd (immune deficiency) that recognize pathogen-associated molecular patterns (PAMPs) and produce antimicrobial peptides (AMPs) to eliminate them (Mahanta et al. 2023). Cellular immune responses like RNA interference (RNAi), melanization, phagocytosis, nodulation, and encapsulation, allow

immune cells to directly attack and sequester harmful pathogens (Vaibhvi et al. 2022). These pathways are differentially triggered by distinct pathogens (Lester et al. 2019). Insects also exhibit individual-level behavioral immune responses, such as self-grooming, which helps remove pathogens from the surface of their bodies (Wilson-Rich et al. 2009). Understanding these immune responses is crucial to understanding host-pathogen crosstalk in social insects.

An important aspect of host-pathogen dynamics is the ability of the pathogen to infect and transmit in the host. Transmission is defined as the ability of the pathogen to enter the host, replicate or disseminate within the host, and pass on to a new host (Louten 2016). Transmission is essential for pathogens to persist across generations of hosts and invade new populations (Schmid-Hempel 1998). On the host side, pathogens can deplete host resources, release toxins, and lead to major fitness effects like reduced lifespan and fecundity. Hence host immune mechanisms are crucial to ensure individual and population-level fitness by limiting pathogen replication and transmission within the colony. Here we use two novel pathogens, one virus and one bacteria, to explore these host-pathogen dynamics in a social insect.

## 1.1 The host

The clonal raider ant, *Ooceraea biroi,* is a queenless ant species with colonies of totipotent female workers (Ravary and Jaisson 2004). Reproduction is asexual through thelytokous parthenogenesis, which results in colony mates being nearly genetically identical (clonal) (Oxley et al. 2014). Reproductive cycles are synchronous with two alternating phases, the foraging and the reproductive phase. Colonies exhibit overlapping reproductive cycles, with eggs being laid while the previous generation is still at the pupal stage (Ravary and Jaisson 2004). The presence of the larvae inhibits ovarian activity and induces foraging in the workers (Ravary et al. 2006; Ulrich et al. 2018). Foraging workers raid the brood of other ant species to feed the developing

larvae (Ravary and Jaisson 2002), which might make them susceptible to pathogen spillovers.

Figure 1 illustrates the potential routes of pathogen transmission within *O. biroi* colonies. The arrows indicate the direction in which the pathogen transfer can occur. Adults can vertically transmit pathogens to the eggs, which may be passed on over subsequent developmental stages. Multiple symbionts are commonly transmitted in this manner (Chaston and Goodrich-Blair 2010). Adult-to-adult transmission may occur through direct physical contact, allogrooming, or handling carcasses of infected ants (Sun and Zhou 2013; LeBoeuf et al. 2016). Trophallaxis, the exchange of fluids between colony members, is a common behavior in many ant species (LeBoeuf 2017). While it has not been reported in *O. biroi*, it might be a potential route of disease transmission. Since adults engage in brood care, infected individuals can transfer pathogens through direct contact with eggs, larvae, or pupae. This is rare in the egg stage due to the protective chorion (Cole et al. 2020). Since workers engage in larval feeding, adult-to-larvae transmission could also be through a food intermediate (Schläppi et al. 2020). Within the developing stages, clustering increases contact, which can facilitate pathogen transfer (Konrad et al. 2012). Infected broods can transmit the pathogen to adults through direct physical contact. Cannibalism of the infected brood (Bizzell and Pull 2024) may also act as a potential route of disease transmission to adults. In addition, ant pupae produce pupal fluid, which might be a potential route of transmission to the adults and the larvae that consume this fluid (Snir et al. 2022). In all the routes represented in Figure 1, the environment could also play an intermediate in pathogen transfer (not shown in figure). In this thesis, we study some of these transmission routes. Due to time constraints and the scope of the study, we have focused on some of the possible routes of transmission highlighted in blue in Figure 1.

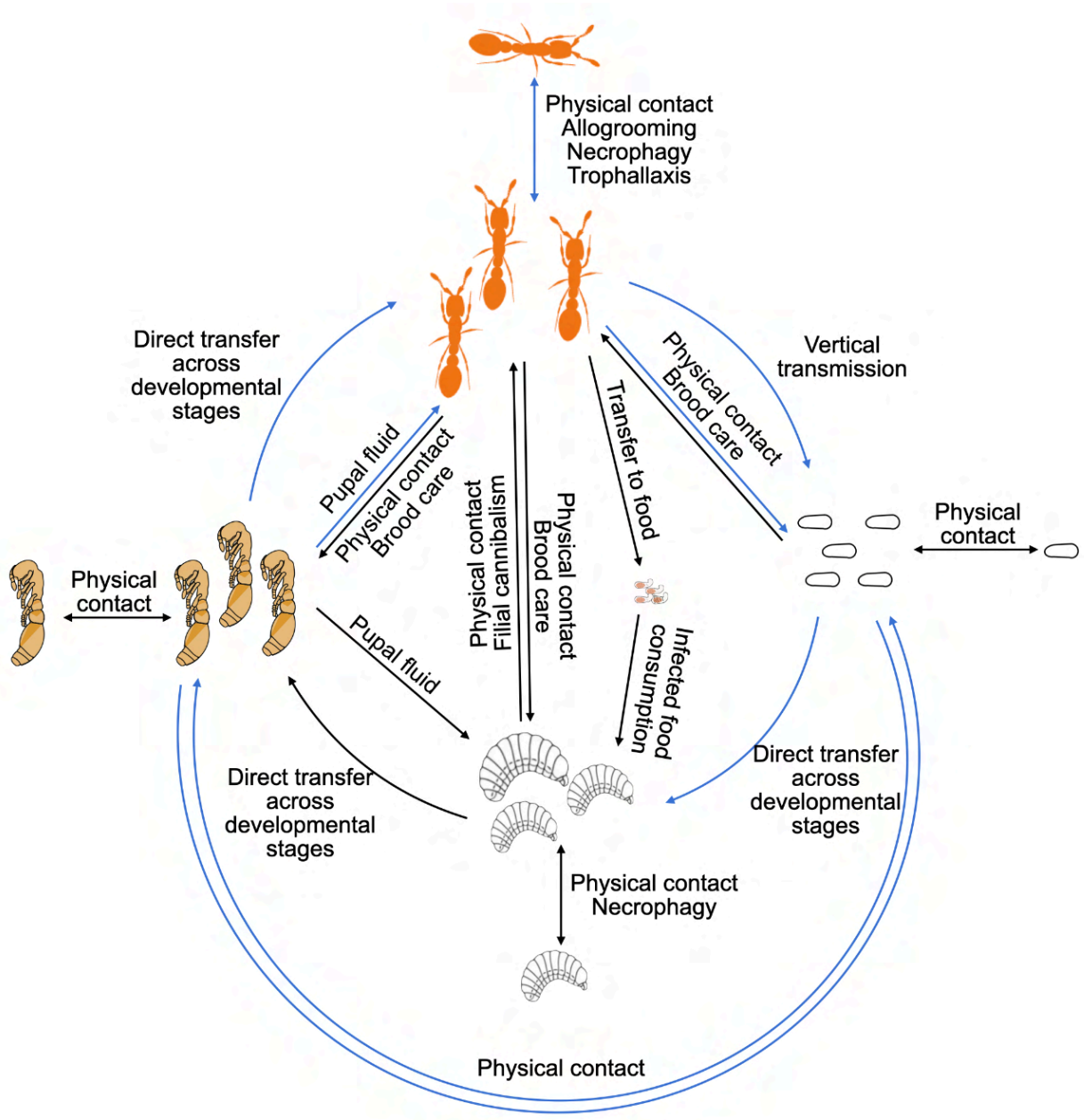


Figure 1: **Routes of pathogen transmission in *O. biroi.*** The symbols in a clockwise direction from the top indicate adult ants, eggs, larvae, and pupae. The direction of the arrow indicates the direction of pathogen transfer. Blue arrows indicate the transfer routes that have been investigated in this thesis.

*O. biroi* is a powerful system to study host-pathogen interactions and immune responses in social insects. Due to their synchronous and clonal reproduction,

experimental control over age and genotype is possible. Age matching is especially important in understanding the effect of pathogens on survival. Additionally, since some studies suggest that genetic diversity limits parasitism, the clonal nature of *O. biroi* colonies may increase their susceptibility to rapid pathogen spread (Gibson 2022). Here we study host-pathogen interaction in *O. biroi* using the acute bee paralysis virus and *Sodalis praecaptivus*.

# 1.2 The pathogens

## 1.2.1 The acute bee paralysis virus (ABPV)

ABPV is a positive sense single-stranded RNA virus frequently found in honeybees, where it causes progressive paralysis, uncontrollable trembling, impaired flight ability, and a gradual darkening of the thorax and abdomen accompanied by hair loss (De Miranda et al. 2010). Recent research found that cross-species transmission of RNA viruses, like ABPV, is possible experimentally and in the wild (Schläppi et al. 2020; Tehel et al. 2022). To date, ABPV has been found in colonies of nine ant species (Baty et al., 2020). However, no associations of ABPV and *O. biroi* have been found by far. Some research indicates that ants might act as reservoirs for honeybee viruses like ABPV (Payne et al. 2020). In *Lasius* spp., foodborne ABPV infection spreads rapidly within the colony and leads to physiological effects, such as reduced foraging speed (Schläppi et al. 2020). Because of ABPV's rapid transmission abilities and its demonstrated effects on ant colonies, we selected this virus to investigate how *O. biroi* colonies respond to viral infection and whether adult-to-adult transmission of the virus occurs within the colony.

Host immune response to ABPV infection is not well understood. In honeybees, no clear evidence of humoral or cellular immune responses to ABPV has been found (Azzami et al. 2012). However, other viruses have been shown to induce RNA interference (RNAi) mediated immune responses in social insects (Flenniken and Andino 2013). The RNAi

pathway is an important immune mechanism that restricts virus replication (and also silences cellular gene expression) by producing small non-coding RNAs called small interfering RNAs (siRNAs) (Gammon and Mello 2015) (Figure 2). Here, we examine whether ABPV infection in *O. biroi* induces an antiviral RNAi response by assessing the expression of *Dicer-2* (*Dcr-2*), a key enzyme in the RNAi pathway. *Dcr-2* is a specialized RNase III enzyme that can bind to foreign double-stranded RNA (dsRNA) and cleave them to form siRNA duplexes that are targeted for degradation (Yamaguchi et al. 2022) (Figure 2). In honeybees, *Dcr-2* upregulation is observed in response to the Sindbis virus (Flenniken and Andino 2013). In ants collected from the wild, *Dcr-2* mediated formation of si-RNA has been observed which is host and virus-specific (Viljakainen et al. 2023). Hence, *Dcr-2* was chosen to understand antiviral immunity in *O. biroi*.

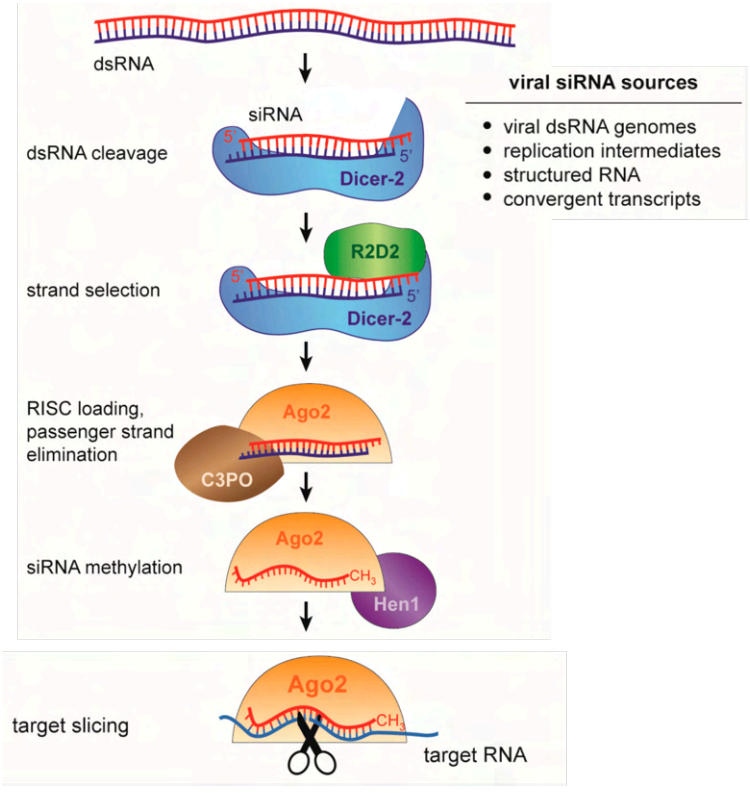


Figure 2: **RNAi Mechanism:** *Dcr-2* binds to different dsRNA sources and cleaves it into ~21 nucleotide siRNA, which are loaded onto Argonaute2 (Ago2), forming the RNAi Silencing Complex (RISC). Here, one strand is degraded, and the other remains attached to Ago2 as a guide strand that mediates recognition of the target RNA through base pairing, followed by target cleavage. R2D2 is a cofactor of Dcr-2. Component 3 Promoter of RISC (C3PO) is an endonuclease that helps in cleavage of the siRNA. Hen1 is an RNA methyl transferase that methylates the 3' terminal of the guide strand, finalizing the maturation of siRNA-loaded RISC. Image adapted from (Schuster et al. 2019)

### 1.2.2 *Sodalis praecaptivus*

*S. praecaptivus* HS is a Gram-stain-negative, non-spore-forming bacteria isolated from the serous fluid collected from a human wound (Clayton et al. 2012). Genomic analysis revealed a close phylogenetic relationship with *Sodalis*-allied endosymbionts associated with a wide range of insect hosts like tsetse flies, weevils, lice, and stink bugs (Chari et al. 2015). Compared to other members of the *Sodalis* genus, it has a larger genome size of 5.16 Mb, is capable of free-living, and can decompose plant and fungal biopolymers, enabling the utilization of diverse carbon sources (Renoz et al. 2024). The presence of *Sodalis* in phylogenetically distant groups suggests that symbiotic relationships with members of this genus arose through independent infectious events like horizontal transfer or environmental acquisition (Clayton et al. 2012). Due to its phylogenetic proximity with commonly found insect endosymbionts, we hypothesize that *S. praecaptivus* would be able to successfully establish infection in *O. biroi,* enabling us to study infection response and transmission dynamics in the host. Additionally, horizontally and vertically transmitting colonies could help us understand how host-pathogen relationships evolve in the spectrum of parasitism to mutualism. Here we use a mutant strain *S. praecaptivus* MC1 to study some of these interactions.

*S. praecaptivus* MC1 is a genetically modified strain of *S. praecaptivus* HS containing a mCherry-zeocin cassette in the lacZ gene, making it fluorescent (Su et al. 2022). Previous research has shown that *S. praecaptivus* MC1 can successfully establish vertically transmissible infection in grain weevils through experimental infection of the eggs (Su et al. 2022). Several members of the *Sodalis*-allied clade have been identified in the bacteriomes of various ant species (Jackson et al. 2022). However, since the microbiome of *O. biroi* has not been characterized, any existing associations between *Sodalis*-allied bacteria and *O. biroi* are unknown. Here we use *S. praecaptivus* to understand the impact of bacterial hosts on fitness and transmission within the colony.

*S. praecaptivus* can produce tyrosine which is an important amino acid for both the host and the bactrium. Bacteria use tyrosine for exopolysaccharide production (necessary for cell aggregation, cell adhesion, biofilm formation, etc), stress response, and DNA metabolism (Grangeasse et al. 2012; Kaur and Dey 2023). Insects require tyrosine for cuticular melanization and sclerotization (Arakane et al. 2016). In multiple insect groups, tyrosine provisioning is crucial for establishment of symbiotic relationships (Wierz et al. 2024). Tyrosine biosynthesis is a common feature among ant-associated symbionts (Jackson et al. 2022). Tyrosine is also an important component of the host immune melanization pathway. Melanization is a conserved humoral immune response present in multiple insects in response to wounding or pathogen invasion (Zdybicka-Barabas et al. 2025). Circulating hemocytes (immune cells in the hemolymph) can detect PAMPs, leading to the synthesis of black melanin in the hemolymph (Figure 3). Melanin encapsulates the pathogen cutting out oxygen and nutrients, thus killing it. Insect hemocytes can also surround pathogens while producing melanin leading to the formation of nodules (Smith et al. 2022). However, melanin formation also releases toxins harmful to both the pathogen and the host. Hence, this response is tightly regulated (Whitten and Coates 2017). Previous studies have found that *S. praecaptivus* might scavenge on host tyrosine resources leading to reduced cuticular melanization (Su et al. 2022). Here we quantify melanization in adult ants and pupae to understand the tyrosine resource partitioning and host immune response, respectively. Since *O. biroi* adults have a thick, melanized cuticle, the measure of cuticular melanization is not sufficient to quantify immune melanin response in the hemolymph. However, since pupae do not have a heavily melanized cuticle we hypothesize that, immune melanization and nodule formation may be visible in pupae.

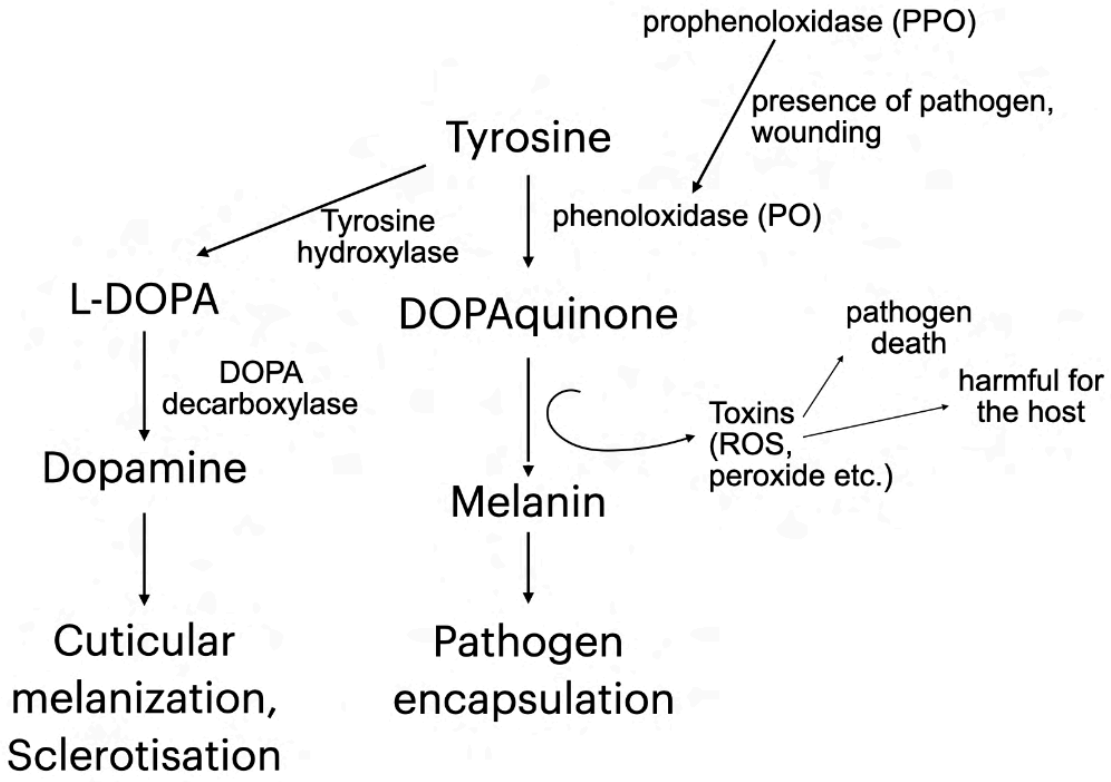


Figure 3 **Simplified melanization pathway in insects:** Tyrosine can be converted to levodopa (L-DOPA) by tyrosine hydroxylase, leading to the formation of cuticular melanin and sclerotization. In the case of immune melanization, circulating hemocytes containing prophenoloxidase (PPO) can detect sites of injury or invading pathogens, causing the release of PPO and subsequent activation of phenoloxidase (PO). PO converts tyrosine to DOPAquinone which gets converted to melanin that can encapsulate pathogen preventing oxygen and nutrient supply to cause death. Toxins like Reactive Oxygen Species (ROS) and peroxide ($H_2O_2$) released in the process facilitate pathogen death but are also harmful to the host. (Anbutsu et al. 2017)

## 1.3 Aims and Objectives

For ABPV, we measure the ability of the virus to successfully replicate in a non-natural host *O. biroi*. Since transmission to new hosts is an important component of successful infection establishment (Louten 2016), we measure adult-to-adult transmission of ABPV

in *O. biroi* colonies using cohabitation assays. Since ABPV is highly virulent in honeybees and has been shown to successfully infect and transmit in ants, we hypothesize that ABPV would successfully replicate in adult ants allowing us to understand virus transmission dynamics in *O. biroi* colonies (De Miranda et al. 2010; Schläppi et al. 2020). To understand the host immune response, we quantify immune gene expression of *Dcr-2* post-injection.

For *S. praecaptivus*, we similarly monitor the ability of the bacteria to replicate in the host. Due to its ability to utilize host resources and successfully establish in insect hosts, we hypothesize that *S. praecaptivus* would successfully infect *O. biroi* (Su et al. 2023). To understand its impact on the host, we measure host survival and fecundity. Since infection dynamics may vary across developmental stages (Searle et al. 2013) we infect various life stages. Different life stages in *O. biroi* colonies are associated with different transmission routes (Figure 1). We use cohabitation assays to monitor several of these routes. To understand the distribution of the bacterium in *O. biroi* adults, we use fluorescence *in-situ* hybridization (FISH) to visualize bacterial localization in host tissues. In addition, we measure melanization responses at different life stages to understand the impact of infection on cuticular melanin formation and immune melanization. Since one of our goals is to develop a system to study how host-pathogen relationships evolve over time in social insects, we aimed to maximize survival and potentially obtain ant colonies of horizontally or vertically transmitting *S. praecaptivus*

Together, our study aims to provide insight into host-pathogen interaction and transmission dynamics in *O. biroi* colonies. The long-term goal is also to use this information to establish horizontally or vertically transmitting host-pathogen systems in *O. biroi* that can be used for experimental epidemiological studies.

# Chapter 2: Materials and Methods

## 2.1 Ant Rearing

All ant colonies were maintained at a constant temperature of 28 °C in airtight plastic containers with a plaster of Paris floor, which was periodically moistened to maintain optimal humidity levels. Colonies in their foraging phase were regularly fed on brood from *Tetramorium bicarinatum, Oecophylla,* and frozen flies sterilized in liquid nitrogen. All the colonies were regularly cleaned and observed under an optical microscope to monitor colony health. Once every four months, colonies were transferred to new boxes with clean plaster to maintain hygienic conditions. All the experiments in this thesis have been conducted with ants of genotype B, which originate from St. Croix, U.S. Virgin Islands (Kronauer et al. 2012).

## 2.2 ABPV infection and transmission dynamics in adults

### 2.2.1 Preparation of viral inoculum

ABPV inoculum was prepared in the lab of Dr. Rober Paxton at the University of Halle, Germany, following the protocols outlined by Tehel et al., 2019. Briefly, 1 µL bee extract obtained from a heavily infected bee, *Apis mellifera,* (identifiable by the darkening of the cuticle and impaired movement), was injected into bee pupae harvested from virus-free colonies. The pupae were allowed to grow for three to five days to allow viral replication and systemic infection. The pupae were homogenized in 0.5 M cold potassium phosphate buffer (PPB, pH 8.0), and the resulting homogenate was screened for the presence of common bee viruses, including DWV-A, DWV-B, BQCV, CBPV, IAPV, SBV, and SBPV, using RT-qPCR. Only homogenates confirmed to contain ABPV exclusively

were used for experiments. Control bee extract was obtained following the same procedure but by injecting bee pupae with virus-free bee extract.

## 2.2.2 Adult microinjection

Ants were immobilized by mounting them on a Läufer Plast 0120 eraser, which was modified with slits to hold the ants in place securely. 10 nL of the viral inoculum was administered into the hemolymph at a controlled rate of 5 nL/s. Injections were performed between tergite IV and V at the posterior end of the gaster using a NanoFil 36 GA beveled needle connected to a UMP3 pump MICRO2T SMARTouch™ controller from World Precision Instruments, USA.

## 2.2.3 Experimental design

**Pilot experiment**

To monitor the time course of viral infection, transmission, and immune response, five randomly selected mixed-aged adult ants of genotype B were injected with 10 nL of ABPV at a concentration of $10^4$ genome equivalents per µL (ge/µL), resulting in an inoculum of 100 ge per ant. An equal number of uninjected adults were introduced into each Petri dish to serve as cohabitating individuals. To differentiate between injected ants and cohabitating ants, the latter were paint-marked using Uni Paint markers (Li et al. 2023). For control, virus-free bee extract was injected using the same procedure. All the ants were housed in a Petri dish of diameter 50 mm with a plaster of Paris floor and provided with *Tetramorium* brood at the start of the experiment. Four replicates, each containing five injected and five cohabitating adults, were set up for every treatment and time point (Figure 5 - A). The five injected and cohabitating ants from each replicate plate were pooled and collected at 0, 6, 12, 24, and 48 hrs post injection (PI), flash-frozen in liquid nitrogen, and stored at -80 °C for RT-qPCR. As part of the initial study, only time points between 0 and 48 hours PI were analyzed for injected ants, while time points at 24 and 48 hours PI were examined for cohabitating ants. These time points were selected based on the hypothesis that viral replication, if occurring, would be most detectable within this timeframe.

**Main experiment**

The findings from the previous experiments highlighted the need for more appropriate control. The use of bee extract as a control may have triggered an immune response, making it difficult to distinguish immune activation due to viral infection from that induced by the bee extract itself. To (a) avoid the impact of age on survival and infection spread, (b) provide an uninjected and unexposed baseline, (c) improve sample size, and (d) verify our results, the previous experiment was repeated with age-matched adults, increased sample size and untreated controls. Three-day-old callow workers were isolated from their parent colony and housed in an airtight plastic container for three weeks to obtain age-matched adults. Six replicates, each containing six adults injected with 100 ge/ant and six cohabitating adults, were set up for every treatment and time point (Figure 6 - A). Based on the previous experiment, time points 0, 12, 24, and 48 hrs PI were selected for sampling. A total of 36 ants were injected for each treatment and timepoint (six ants/plate). Uninjected ants, unexposed to the ABPV, were used as baseline controls for viral load and immune gene expression. The rest of the protocol was similar to the pilot experiment.

## 2.2.4 RNA Extraction and RT-qPCR

Samples stored at -80 °C were immersed in 1 ml TRIzol with two stainless steel beads, homogenized for 2 min using a Qiagen TissueLyser II, frozen on dry ice, and thawed. This process was repeated three times to optimize tissue lysis. Total RNA was extracted using the Qiagen Rneasy Mini Kit following the manufacturer's protocol with minor modifications to increase yield. RNA was eluted in 20 µL nuclease-free water from Sigma Aldrich. The elution step was repeated twice to maximize yield. RNA concentration and purity were assessed using an Eppendorf BioPhotometer™ D30. For cDNA synthesis, 200 ng of total RNA was reverse-transcribed using M-MLV Reverse Transcriptase (Promega) following the manufacturer's instructions. The cDNA thus obtained was diluted three times and stored and -20 °C.

qPCR was performed using the KAPA SYBR® FAST Universal kit according to the measurements listed in Table 1. A 364-well plate was set up consisting of technical duplicates for each sample and a no-template negative control.

To quantify the exact number of genome equivalents present in the ant samples, a standard curve (S1, supplementary) was obtained by extracting RNA from the viral inoculum, followed by cDNA synthesis and PCR amplification using *Taq* polymerase (New England Biolabs). PCR was performed following the manufacturer's protocols. The PCR product was verified using gel electrophoresis on a 2% agarose gel. The resultant band was cut out and purified using the Nucleospin Gel and PCR Purification kit following the manufacturer's instructions. The DNA obtained was quantified using a BioPhotometer, and several 1:100 dilutions were made. This was then used to make serial dilutions of $10^{12}$. The standard curve thus obtained was tested before being used for quantitative analysis.

To quantify expression levels of immune gene *Dcr-2* in the experimental samples, relative expression levels were measured compared to the housekeeping gene *ribosomal protein L13a* (*RPL-13a*) as a reference. *RPL-13a* is a component of the 60S large ribosomal subunit involved in protein synthesis and is stable across tissue types and conditions in insects (Oxley et al. 2014). All the qPCRs were performed using QuantStudio™ 5, and all PCRs were performed in an Applied Biosystems Veriti™ Thermal Cycler. Detailed protocols for all the reactions have been described in Table 1. All the primers have been listed in Table 2.

## 2.2.5 PCR for negative sense strand detection of ABPV

Since ABPV is a positive sense RNA virus, viral replication requires the formation of the negative strand. Hence, the detection of the negative sense strand is an indicator of the replicative status of the virus in the host (Schläppi et al. 2020). cDNA synthesis was performed using Superscript® III reverse transcriptase since it helps avoid false positives due to its efficiency at high temperatures (Craggs et al. 2001). cDNA was

obtained using a tagged primer. The reaction mix was cleaned up using NucleoSpin® Gel and PCR Clean-up kit (Marchery Nagel, Oensingen, Switzerland) and eluted in 20 µL elution buffer and 1:3 elution was used for PCR amplification using *Taq* polymerase (Table 1). A tag oligonucleotide complementary to the tagged primer used for cDNA synthesis was used as a forward primer (Table 2), and a corresponding reverse primer was used. To ensure all the tagged primers were removed in the purification process, one control with only the reverse primer was set up for each sample. Resultant PCR products were verified by gel electrophoresis on a 2% agarose gel and visualized under UV light with a 1kb ladder (New England Biolabs) as reference.

As a positive control for the experiment, mixed-aged honeybee pupae (*A. mellifera)* were injected with the viral inoculum and the clean bee extract. The pupae were reared at 37$^{o}$C for 5 days and sacrificed for RNA extraction. This also allowed us to verify the purity of the clean bee extract. Contamination in the clean bee extract would lead to viral replication in their natural bee hosts.

| **Reagent** | **1x** |
|---|---|
| Protocol for qPCR | |
| KAPA SYBR® Reaction mix | 3 µL |
| Forward Primer (FP) | 0.12 µL |
| Reverse Primer (RP) | 0.12 µL |
| Water | 1.25 µL |
| cDNA | 1.5 µL |
| Total reaction volume | 6 µL |
| 3 min incubation at 95°C; 40 cycles of 10 s at 95°C, 30 s at 57°C, 20s at 72°C; final elongation at 95°C, Melt curve analysis from 55°C to 95°C with 0.5°C increments per second | |
| Protocol for cDNA synthesis of negative strand detection | |
| Tagged primer | 1 µL |
| dNTP | 1 µL |
| RNA | 200 ng |

| | |
|---|---|
| Water | (10 - volume of RNA) µL |
| 5 min incubation at 65°C; | |
| 5x Buffer | 4 µL |
| O.1 M DTT | 1 µL |
| Superscript III | 1 µL |
| Water | 1 µL |
| Total Reaction volume | 20 µL |
| 55 min incubation at 65°C; 15min at 70°C | |
| PCR protocol for negative strand amplification<br>PCR protocol for viral amplification for standard curve preparation | |
| 10x buffer | 2.5 µL |
| Water | 15.75 µL |
| dNTP (10mM) | 0.5 µL |
| FP | 0.5 µL |
| RP | 0.5 µL |
| Taq polymerase | 0.125 µL |
| cDNA (1:3 diluted) | 2.5 µL |
| Total Reaction volume | 23 µL |
| 3 min incubation at 95°C; 35 cycles of 20 s at 95°C, 20 s at 56°C, 30s at 68°C; 2 mins at 68°C | |

Table 1. **PCR protocols for the different types of PCRs:** The grey column refers to the purpose of the PCR. This is followed by a detailed description of the reaction mixture used and the thermal cycling profile.

| **Primers used for RT-qPCR of ABPV** | |
|---|---|
| FP | catggctcaagacacttcatcg |
| RP | ccagcaatgacctcaatgtgg |
| **PCR for virus amplification for standard curve** | |

| | |
|---|---|
| FP | catggctcaagacacttcatcg |
| RP | ccagcaatgacctcaatgtgg |
| **Primers used neg-strand specific cDNA symthesis of ABPV** | |
| Tagged FP | agcctgcgcaccgtggttggtttggtgcagaaggtg |
| **Primers used neg-strand specific PCR of ABPV** | |
| FP (Tag) | agcctgcgcaccgtgg |
| RP | agaaaagtccataggcccgt |
| **Primers used for *Dcr-2* qPCR** | |
| FP | ctcggtggatcggcgaaata |
| RP | tgaggttcacgatcatcgcc |
| **Primers used for *RPL-13a* qPCR** | |
| FP | gcaaacaaaagcgtgtcaag |
| RP | tcggccagagtaaaacctct |

Table 2. **List of primers used for various experiments.** The specific experiment for which the primers were used is labeled on the top in bold.

# 2.3 *S. praecaptivus* MC1 infection response and transmission dynamics in adult *O. biroi*

## 2.3.1 Preparation of the inoculum for experiments

*S. praecaptivus* MC1 from the glycerol stock was inoculated into 20 ml LB broth in a 50 mL falcon tube under the sterile hood and grown overnight for 18-19 hrs at 30°C and 180 rpm (Su et al. 2023). The bacterial culture was centrifuged at 3000 rpm for 10 minutes to pellet the cells. The pellet was washed with an equivalent volume of phosphate-buffered saline (PBS) to remove residual media. Subsequently, the pellet was resuspended in 750 µL of PBS to prepare the bacterial suspension. Serial 10-fold dilutions of the bacterial suspension were performed up to a dilution factor of $10^4$. The

$10^1$ dilution was used to measure optical density (OD) with an Eppendorf BioPhotometer™ D30, using PBS as the blank standard.
For cell counting, the $10^4$ dilution was examined using a Neubauer Improved hemocytometer under a Leica DMi1 microscope at 40x magnification. Cells visible within five squares (including only the right and the bottom boundaries of the square) of 0.04 mm² along the diagonal of the grid on both sides of the counting chamber were enumerated. The procedure was repeated three times, and the average of all six readings was calculated to ensure consistency and accuracy. Prior to each count, the bacterial suspension was vortexed for one minute to ensure a uniform distribution of cells. The final concentration of bacterial cells in the original suspension was calculated using the formula:

$$Cells\ per\ \mu L\ of\ the\ original\ sample\ = \frac{Number\ of\ cells\ counted}{Surface\ area\ counter(in\ mm^2) \times Depth\ of\ the\ Chamer(mm) \times\ Dilution\ factor}$$

$$Cells\ per\ \mu L\ of\ the\ original\ sample\ = \frac{Number\ of\ cells\ counted \times 10000}{5 \times 0.04 \times 0.01 \times 1}$$

This procedure was repeated prior to every experiment involving *S. praecaptivus*. For each round of cell counting, the number of cells per microliter was calculated at OD = 1 as a validation step to minimize counting errors. Across all injection rounds, a consistent cell density of approximately $2.5 \times 10^7$ cells/µL was obtained at OD = 1.

### 2.3.2 *S. praecaptivus* MC1 injection in adults

To monitor infection spread, dosage response, mortality, and vertical and horizontal transmission of the bacteria in the host, age-matched adult ants, four weeks post eclosion, were injected with *S. praecaptivus* MC1. Preliminary experiments indicated that the injection of approximately 2000 bacterial cells resulted in 50% mortality at 7 days post-injection (DPI). Based on these findings, two dosages, 2000 cells/adult (2K) and 1000 cells/adult (1K), were selected to minimize mortality among the ants. Microinjection was done following the protocol detailed in Section 2.2.2. Bacterial

inoculum of 2 x $10^5$ µL and $10^5$ µL were prepared, and 10 nL was injected into the hemolymph of each ant for 2K and 1K dosage, respectively. Control injections were done using PBS. Post-injection, eight injected ants were placed in Petri dishes (50 mm diameter) with a plaster of Paris floor to maintain humidity. Four uninjected, cohabitating adult ants were added to each plate and identified by marking their gasters with paint (section 2.2.3). Twelve replicates were set up for each treatment (n = 98 injected ants per treatment, n = 48 cohabitating ants per treatment). Four plates of 12 uninjected ants of the same age per plate were additionally set up as sham controls (n = 48 ants). All the plates were cleaned, watered, and provided with food every day and maintained at 27°C. Mortality was recorded daily from DPI-1 to DPI-14. Ants confirmed to be dead were removed each day using cotton swabs. The entire experiment was conducted in two blocks of six replicates each.

An additional replicate was set up, which was imaged for fluorescence intensity each day until DPI-7 using a Leica M165 stereomicroscope to monitor infection spread. Since this replicate was subjected to frequent disturbance, it was not included in the mortality measurements. mCherry fluorescence was used to measure the infection spread, which allowed long-term monitoring without sacrificing the ants. Eggs were collected and counted at DPI-7 from each colony across all replicates (12 plates per treatment). Collected eggs were measured for fluorescence intensity to detect possible vertical or horizontal transmission from the cohabitating infected adults. At DPI-8, all adult ants (except the sham) we subjected to measurement of fluorescence and melanization to determine infection status and potential transmission to the non-injected cohabitating adults. One of the replicates from the PBS-injected ants and the 2K *S. praecaptivus* injected ants were sacrificed at DPI-9 to obtain ants for FISH. These replicates were excluded from the mortality measurements but included in all other readouts.

### 2.3.3 FISH

The localization of *S. praecaptivus* in *O. biroi* was investigated using FISH. Four adults injected with a 2K dosage were used at DPI-9. The infection status was confirmed by

verifying mCherry fluorescence prior to sacrificing the samples. For control, four uninjected and four PBS-injected ants were used. Whole mount FISH was performed following the methods described by (Weiss and Kaltenpoth 2016). In brief, samples were fixed overnight using a Formaldehyde solution (1 ml of 40% paraformaldehyde in 9 mL of 90% tertiary butanol). The legs of the whole insect were removed, and the samples were pre-embedded in 1% agar following three washes in 80% butanol for 30 mins. Dehydration was performed overnight using progressively increasing concentrations of butanol. Dehydrated samples were embedded in Technovit 8100, and 5 µm sections were made using the microtome (Leica HistoCore Autocut R) with glass blades. The sections were transferred to glass slides, and hybridization was carried out at 50°C for 24 hours in a hybridization buffer (0.9 M NaCl, 0.02 M Tris-HCl, pH 8.0, and 0.01% SDS) containing 25 nM each of *Sodalis* specific probe (Cy3-5'-TCCGCTGACTCTCGCGAGAT-3'), a general 16sRNA probe (Cy5-5'-GCTGCCTCCCGTAGGAGT-3') for all eukaryotic bacteria and counterstained with 1 µL of 0.5 mg/mL DAPI (4',6-diamidino-2-phenylindole) (Weiss et al. 2025). This was followed by two washes in pre-heated wash buffer at 50°C, followed by two washes in distilled water. 30 µL Vectashield® Plus (Vector, Burlingame, USA) was used to place the coverslip. One ant of each treatment was imaged using the Leica THUNDER imager DMi8 (Leica, Wetzlar, Germany), and the rest was kept for future imaging.

### 2.3.4 *S. praecaptivus* MC1 egg Injections and rearing

Eggs were injected to monitor infection progression across life stages and to establish a vertically transmissible line of *S. praecaptivus* in *O. biroi*. A bacterial inoculum of ~25 cells/nL was used for egg injections. This concentration was chosen based on a pilot conducted before the main experiment that led to the successful hatching of the eggs into larvae and previously tested concentrations in *Drosophila melanogaster,* which, like *O. biroi,* are non-natural hosts of *S. praecaptivus* (Su et al. 2023). Egg-laying units were available in the lab consisting of 60-80 *O. biroi* adults (genotype B) housed at 27°C in Petri dishes of radius 5 cm, with a thin layer of plaster of Paris floor, and fed three times a week. Since previously laid eggs are observed to inhibit egg production in *O. biroi*

(Trible et al. 2017), eggs were collected one day before injection to synchronize the egg-laying cycles in the laying units. Egg collection was done using a paintbrush to incur minimal damage due to handling. Freshly produced eggs over the next 24 to 48 hrs were collected on the injection day.

An agar plate prepared by mixing 0.2 g LB agar with 10 mL of water was used to mount the eggs for injection. *O. biroi* eggs are pointier on the posterior end compared to the anterior and slightly concave on the ventral side compared to the convex dorsal surface. Given that the nucleus is positioned closer to the anterior end, injections were performed at the posterior end to minimize mortality caused by injection-induced damage. For precise alignment, grooves were made on a Whatman filter paper (Cytiva) using a sharp blade. Eggs were then arranged within these grooves, with their posterior ends facing outward and their dorsal sides oriented upwards. To maintain hydration and prevent displacement during the injection process, the filter paper was periodically moistened with distilled water. A coverslip was placed over the filter paper to secure it in position, and it also served as a tool for breaking the tip of the glass capillary used for injection. Using this setup, approximately 200 eggs could be injected in a single experimental round.

Microinjections were performed using a manual microinjector operated with compressed nitrogen ($N_2$) at a pressure of 4 bar under a Zeiss Discovery V8 stereomicroscope. Glass capillaries (Science Products, Germany) were pulled using a Flaming Micropipette Puller (Sutter Instrument Co, USA) using settings: heat 515, pull: 30, velocity: 70, time: 250, was used for injecting the eggs. The inoculum was vortexed for one minute before loading into the capillary. The capillary was verified for blockage at the start of the injections and at frequent intervals during the injection. In case of blockage, it was replaced with a new capillary before the injections were continued. This protocol was adapted from the established microinjection method for *O. biroi* eggs (Trible et al., 2017)and refined based on the microinjection protocol for *S. praecaptivus* in grain weevil eggs (Su et al. 2023).

Following injection, the individual eggs were placed in Petri dishes and monitored every day until all the eggs were dead or hatched into larvae. Eggs displaying fungal growth, abnormal physical form, or excessive fluid surrounding them were removed using a paintbrush, and the area was cleaned with 70% ethanol to avoid further growth of fungi. The moisture in the Petri dish was maintained by providing a few droplets of water on the inverted cap of an Eppendorf tube stuck to a corner of the Petri dish using adhesive. Approximately 100 uninjected eggs were placed as incubation controls. All the plates were placed in plastic containers lined with wet tissue paper to maintain moisture and kept at 27°C.

Upon hatching, each larva was individually checked for fluorescence before being placed with callows for further development (Trible et al. 2017). Each rearing unit consisted of ~30 2-3 day old callows placed with ~30 mixed larvae from injected and control plates. The rearing units were periodically checked under the microscope to monitor the presence of fluorescence in the larval cluster within the colony. All the rearing units were regularly fed on the brood from *Tetramorium* and maintained at 27°C.

### 2.3.5 Pupae injection with *S. praecaptivus* MC1

To monitor the impact of infection spread in pupae and transmission dynamics to cohabitating adults and eggs, 3 - 4 day-old pupae were injected with *S. praecaptivus.* Pilot studies showed that microinjection with a bacterial inoculum of 25 cells/nL was sufficient to establish infection in pupae. Based on these results, two dosages, 25 cells per nL (25 cpn) and 10 cells per nL (10 cpn) were chosen to minimize mortality while ensuring infectivity in the pupae. Pupae were microinjected using glass capillaries, as described in Section 2.3.4. Since pupae are comparatively larger, a handheld pair of forceps was used to stabilize them instead of the agar plate with filter paper. Six replicates of six injected pupae (n = 36 per treatment) placed in a plastered Petri dish (prepared similarly to section 2.3.2) with 8 non-injected cohabitating adults (n = 48 per treatment) were prepared for each treatment. As a control, pupae were injected with PBS. All the replicates were maintained at 27$^{o}$ C and monitored over 16 days. Two

replicates of six uninjected pupae with eight adults were additionally set up as sham controls (n = 12 for pupae, 16 for adults). An additional replicate was set up, which was imaged for fluorescence intensity each day until DPI-4 to monitor infection spread. Since this replicate was subjected to frequent disturbance, it was not included in the mortality measurements. At DPI-4, all pupae (except the sham) we subjected to measurement of fluorescence and melanization to determine infection status. At DPI-16, eggs laid by the cohabitating adults in this duration were collected from each replicate and imaged to detect the horizontal spread of bacteria. Simultaneously, all the cohabitating ants were also images to monitor adult-to-adult transmission.

### 2.3.7 Image analysis

Images for fluorescent intensity and melanization quantification were taken using a Leica M165 Leica M165 stereomicroscope under fixed configurations (Table 3). All the images were captured at maximum LED illumination with the iris 100% open.
Adult ants were imaged by immobilizing them on a Läufer Plast 0120 eraser by placing them under a nylon thread for quantitative comparisons. Representative images, only for visualization, were taken by immobilizing adults on a cold plate. Both the eraser and the cold plate were painted in Culture Hustle's Black 4.0 paint for maximum contrast. Since the egg, larval, and pupal stages are stationary, images were captured by placing them on a glass slide with black printed paper in the background.
Images were analyzed using the ImageJ software (Collins 2007). The mean intensity (∑ grey values of each pixel/number of pixels) was measured for different regions, as listed in Table 3 (Schindelin et al. 2012). Due to antenna movements, sometimes both antennae were not on the focal plane. In that case, only the in-focus antenna was used for analysis. When both antennae were in focus, the average of the mean intensity of both antennae was used for analysis (∑ mean intensity of antennae/2). For cohabitating adults, since the gaster was painted, only the antenna was used for fluorescence measurements. The head was excluded from the analysis since some portions of the head were found to be autofluorescent.

| Specimen | Function | Magnification | Exposure | Gain | Areas used for analysis |
|---|---|---|---|---|---|
| Adult | Fluorescent Intensity | 2 | 375.5 | 420 | Antennae, thorax, Gaster |
| Adult | Melanization | 2 | 24.5 | 280 | Head, thorax, gaster |
| Painted Adult | Fluorescent Intensity | 2 | 375.5 | 420 | Antennae |
| Pupae | Fluorescent Intensity | 2 | 168.5 | 400 | Whole body |
| Pupae | Melanization | 2 | 23 | 210 | Whole body |
| Egg | Fluorescent Intensity | 6.3 | 151 | 400 | Whole body |

Table 3: Details of the imaging configurations of various experiments. For a particular life stage, the same configuration was used across all the experiments.

## 2.4 Statistical analysis

Data analysis was performed using RStudio 4.1.2. For survival analysis, the Schoenfeld residuals test was used to assess the proportional hazards assumption in Cox regression models. If the proportional hazards assumption was valid, the Cox proportional hazards model was used for survivability analysis (package *coxme*). Based on the results of the Schoenfeld residuals test, both the ABPV survival datasets were analyzed using *coxme*, using the experimental plates as a random factor and groups as a fixed factor (groups indicate a combination of treatment and injected or cohabitating status. eg ABPV injected ants are a group and corresponding cohabitating ants are a separate group). For the preliminary experiment, the bee-extract injected ants were used as a baseline. For the main experiment, the untreated controls were used as the baseline. Pairwise comparisons for all the groups, were performed using pairwise

log-rank tests (package *survival*) with Benjamini-Hochberg correction. For both the datasets with *S. praecaptivus* the proportional hazards assumption was not valid. Hence, the Accelerated Failure Time (AFT) model with Weibull distribution (package: *survival*) was used with experimental groups as the fixed factor and untreated ants as baseline. Pairwise comparisons were performed using pairwise log-rank tests (package *survival*) with Benjamini-Hochberg correction. For all the datasets, survival was visualized using the Kaplan-Meier survival curves.

For all the experiments (except survival measurements), statistical analysis was done separately for injected and cohabitating groups. For the qPCR and fluorescent intensity measurements, the normality of the data was verified using the Shapiro-Wilk test (package: *stats*). Among the normally distributed datasets, those involving measurements across time points were analyzed using a two-way analysis of variance (ANOVA) with the interaction between treatment and time points (package: *stats*). For datasets involving measurements at one time point, one-way ANOVA was used (package: *stats*) with treatment as the main effect. Pairwise comparisons were made using Tukey's post hoc test.

For non-normally distributed data, the Scheirer-Ray-Hare test was performed with interaction between time points and treatment for datasets involving measurements over time. Pairwise comparisons following the Scheirer-Ray-Hare test were conducted using the Wilcoxon rank-sum test with Bonferroni correction (*rstatix* package). For datasets involving measurements at one time point, the Kruskal-Wallis test was used with treatment as the main effect, followed by Dunn's post hoc test with Bonferroni correction was used for pairwise comparisons (FSA package).

*Dcr-2* expression data was analyzed using the double delta Ct method (Livak and Schmittgen 2001). Statistical analysis was performed on the $\Delta CT$ ($Ct_{target}$-$Ct_{houskeeping}$) values obtained with respect to the housekeeping gene.

# Chapter 3: Results

## 3.1 ABPV infection response and transmission dynamics in *O. biroi*

### 3.1.2 Preliminary Experiment to monitor ABPV infection

To understand the impact of ABPV on the survival of *O. biroi,* mortality was monitored for 48 hrs PI. No differences in survival between ants injected with the virus and those injected with clean bee extract (Cox proportional hazards model: Bee-extract.I v/s ABPV.I: ($\beta$) = 0.56, $p$ = 0.14, Figure 4 - B where Bee-extract.I represent ants injected with clean bee extract, ABPV.I represent ants injected with the viral inoculum, n = 20 for both). No significant differences were observed between the cohabitating groups (Bee-extract.CH v/s ABPV.CH: ($\beta$) = 0.56, $p$ = 0.14, where Bee-extract.CH represents ants cohabitating Bee-extract.I, ABPV.CH indicates ants cohabitating ABPV.I, n = 20 for both). Overall, survival was high, with approximately 80% of ants surviving throughout the experiment (Figure 4 - B). This was expected due to the low dosage chosen to ensure sustained infection while maintaining the ants' viability for subsequent immune response analysis.

qPCR revealed no increase in viral load over time (Figure 4 - B, C). Among ants injected with ABPV, no differences across time points (Bee-extract.I: n = 4, ABPV.I: n = 4, Scheirer–Ray–Hare test, $H$ = 1.49, $p$ = 0.68), treatments ($H$ =0.095, $p$ = 0.75) or their interaction ($H$ =0.08, $p$ = 0.99) were observed. Among the cohabitating ants too, no differences were observed (Bee-extract.CH: n = 4, ABPV.CH: n = 4, Two way ANOVA, main effect, Treatment: $F(1,11) = 2.02$, $p$ = 0.18, Timepoints: $F(1,11) = 1.49$, $p$ = 0.25; interaction $F(1,11) = 0.18$, $p$ = 0.67). Together these results indicated that viral loads remained unchanged over time in injected ants and were not transmitted to cohabitating adults.

The absence of an increase in viral load could have been due to the elimination of the virus by the immune system. Hence, the expression of the immune gene *Dcr-2* was measured in all experimental groups. *Dcr-2* expression levels varied significantly across time points in injected ants (Bee-extract.I: n = 4, ABPV.I: n = 4, Scheirer–Ray–Hare test, $H = 11.12$, $p = 0.03$), but no differences were observed between treatment groups ($H = 0.16$, $p = 0.69$) or their interaction ($H = 0.16$, $p = 0.12$) (Fig. 4 - E). Among cohabitating ants, no significant differences were observed ((Bee-extract.CH: n = 4, ABPV.CH: n = 4, Two way ANOVA, main effect, Treatment: $F(1,9) = 0.89$, $p = 0.37$, Timepoints: $F(1,9) = 1.13$, $p = 0.31$; interaction $F(1,9) = 3.73$, $p = 0.09$; Figure 4 - F). These results indicated a change in *Dcr-2* over time but no change across treatments.

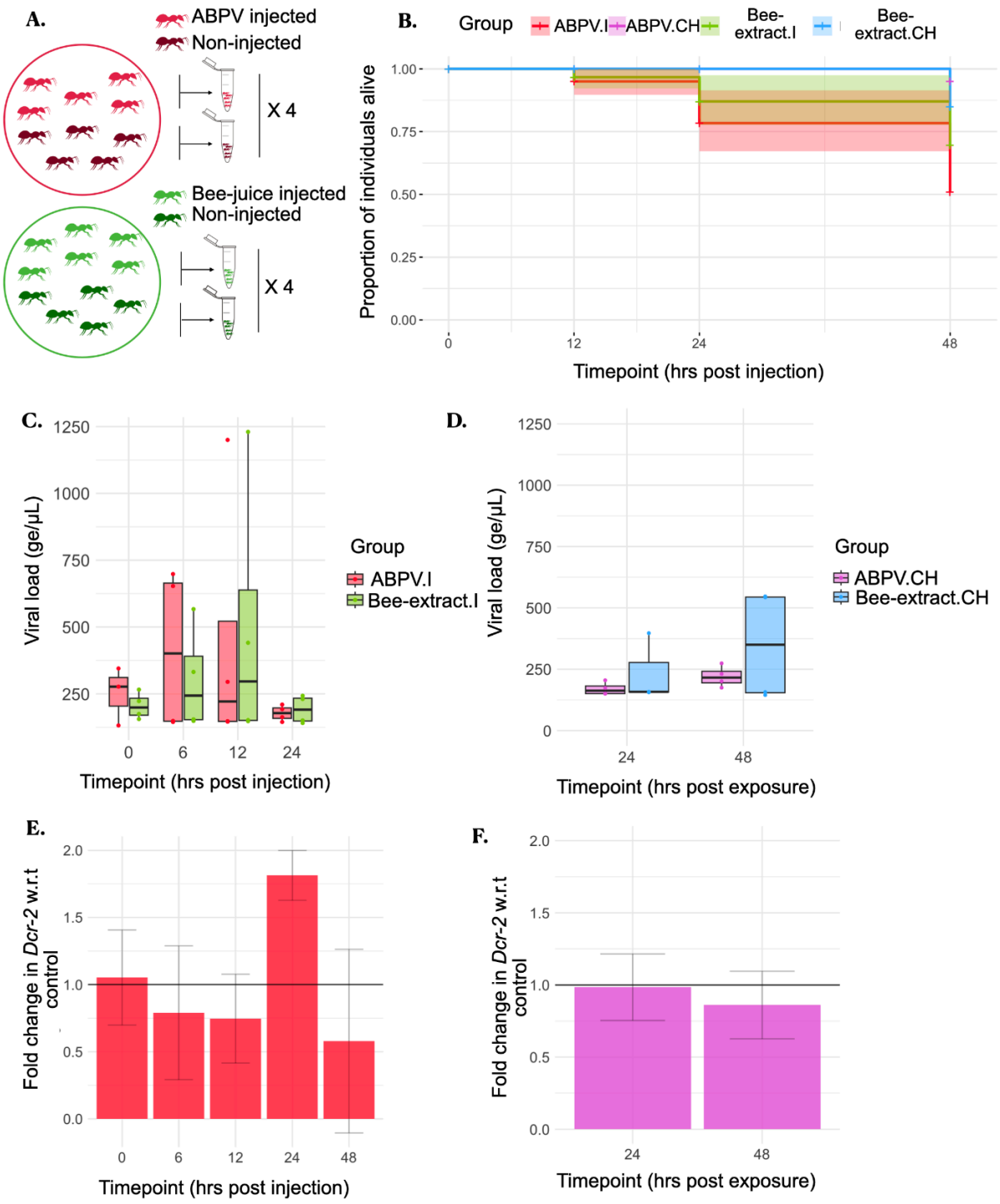


Figure 4: **Preliminary experiment to determine ABPV infection in *O. biroi*** (A) Schematic representation of the experimental design (B) Kaplan-Meier survival curves, shaded regions indicate the 95% confidence interval for survival probability at each time point (n = 20 ants per group) (C) Viral load in injected ants (D) Viral load in cohabitating

ants, the y-axis represents hours post-exposure to injected ants (E) Relative expression levels of *Dcr-2* in ABPV-injected ants compared to bee-extract-injected control ants. (F) *Dcr-2* expression levels in ants cohabitating with ABPV-injected individuals, compared to those cohabitating with bee-extract-injected ants; the y-axis represents hours post-initial exposure to injected ants; Box plots represent the median (central line) and the 25% and 75% quantile of the data (upper and lower lines of the box), with whiskers extending to the minimum and maximum values within 1.5 times the interquartile range.

## 3.1.2 Main experiment

**Impact of ABPV infection on fitness**

To assess the impact of ABPV on survivability, mortality was measured over 48 hrs PI. Survivability analysis was done with the untreated individuals as the baseline, and revealed a significant increase in mortality in all the injected groups (Cox Proportional Hazards model, ABPV.I: ($\beta$) = 0.74, $p < 0.01$; Bee extract.I: ($\beta$) = 0.66, $p<0.01$, Figure 5 - B). No differences in mortality were observed in the cohabitating groups compared to the untreated group (ABPV.CH: ($\beta$) = 0.90, $p = 0.34$; Bee extract.CH: ($\beta$) = 0.85, $p = 0.14$; Figure 5 - B). Pairwise comparisons revealed no differences between injected ants (ABPV.I v/s Bee-extract.I: $p = 0.51$) and the cohabitating ants (ABPV.CH v/s Bee-extract.CH: $p = 0.84$). These results confirm that a dosage of 100 ge of ABPV does not significantly affect survival in *O. biroi* (Figure 5 - B).

**Time-course change in viral load**

qPCR to monitor the change in viral loads over time revealed no significant differences across time points (Scheirer–Ray–Hare test, Bee-extract.I: n = 6, ABPV.I: n = 6, Untreated: n = 6, $H = 5.97$, $p = 0.11$, Figure 6 - C) or treatment ($H = 3.72$, $p = 0.15$) or their interaction ($H = 12.5$, $p = 0.05$). Among the cohabitating ants, a significant increase in viral load was observed across treatments (Two way ANOVA, Bee-extract.CH: n = 6, ABPV.CH: n = 6, main effect, Treatment: $F(1, 27) = 5.11$, $p = 0.03$, Timepoints: $F(2, 27) = 0.88$, $p = 0.43$; interaction $F(2, 27) = 1.18$, $p = 0.32$). Post hoc comparisons revealed a significant increase in the ABPV.CH group at 24 hrs compared to the Untreated ($p =$

0.046). To further confirm the replication status, a negative-sense strand-specific RT-PCR was performed.

To detect viral replication, three samples corresponding to the highest viral loads across all groups (n = 6 per group per time point) at 24 hrs PI were selected for this analysis. As honeybees are the natural hosts of ABPV, bee pupae injected with ABPV were included as a positive control.

The results revealed the absence of viral replication in all the injected and cohabitating groups. The replicative strand was detected in the ABPV-injected honeybee pupae, identified by a strong 200 kb fragment (Figure - 6). No such fragments were detected in any of the other samples, including ants from all treatment groups. Additionally, the absence of the negative strand in the bee pupae injected with clean bee extract confirmed the purity of the control inoculum. No fragments were observed in the cDNA purification controls, confirming that the results were not due to contamination or false positives. These findings suggest that ABPV neither replicates nor transmits in colonies of adult *O. biroi*. The small differences observed in the qPCR were likely due to background noise rather than actual variation in viral load.

To further investigate the possibility of elimination of the virus through RNAi, *Dcr-2* expression levels were quantified. Similarly to the previous results, *Dcr-2* levels were found to change significantly across time points, but no significant differences were observed across treatments (Two way ANOVA, main effect, Treatment: $F(2, 52) = 1.45$, $p = 0.24$, Time points: $F(3, 52) = 3.45$, $p = 0.03$; interaction $F(6, 52) = 1.35$, $p = 0.25$; Figure 5 - D). Tukey's post hoc revealed no significant differences in *Dcr-2* across treatment groups compared to the uninjected control (Figure 5 - D). In the cohabitating groups, no significant differences across treatments and timepoints (Two way ANOVA, main effect, Treatment: $F(2, 40) = 2.86$, $p = 0.07$, Timepoints: $F(2, 27) = 0.32$, $p = 0.73$; interaction $F(4, 27) = 4.26$, $p = 0.005$). These results indicate the lack of a *Dcr-2*-induced immune response.

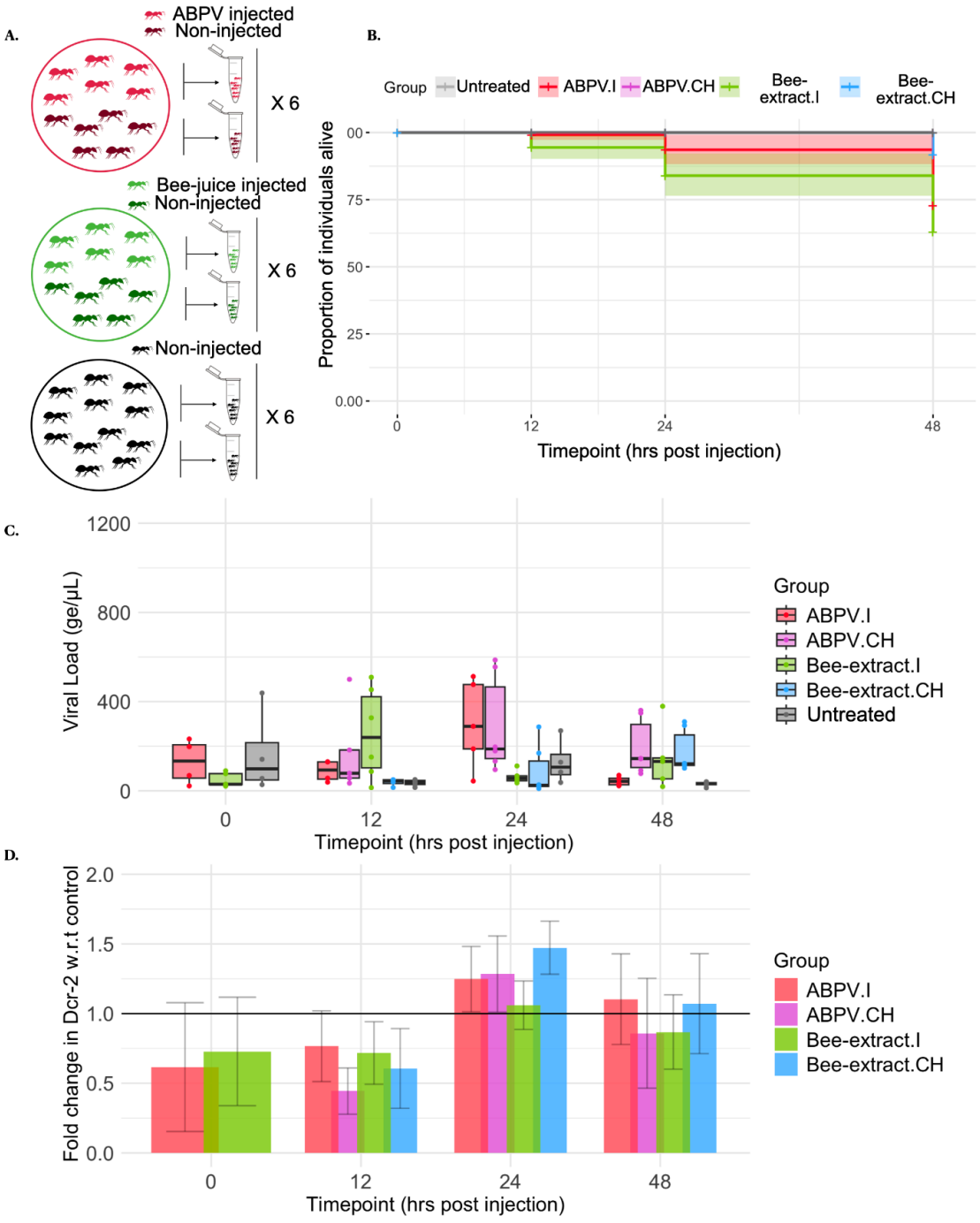


Figure 5 **Replication, transmission, and survival effects ABPV on *O. biroi*** (A) Experimental Design (B) The Kaplan-Meier survival curves with shaded region indicate a 95% confidence interval of the survival probability at each time point (n = 36 ants per group) (C) Viral load in the ants (D) *Dcr-2* expression levels w.r.t untreated adults; Error bars in (C) and (D) represent mean ± SEM. Box plots represent the median (central

line) and the 25% and 75% quantile of the data (upper and lower lines of the box), with whiskers extending to the minimum and maximum values within 1.5 times the interquartile range.

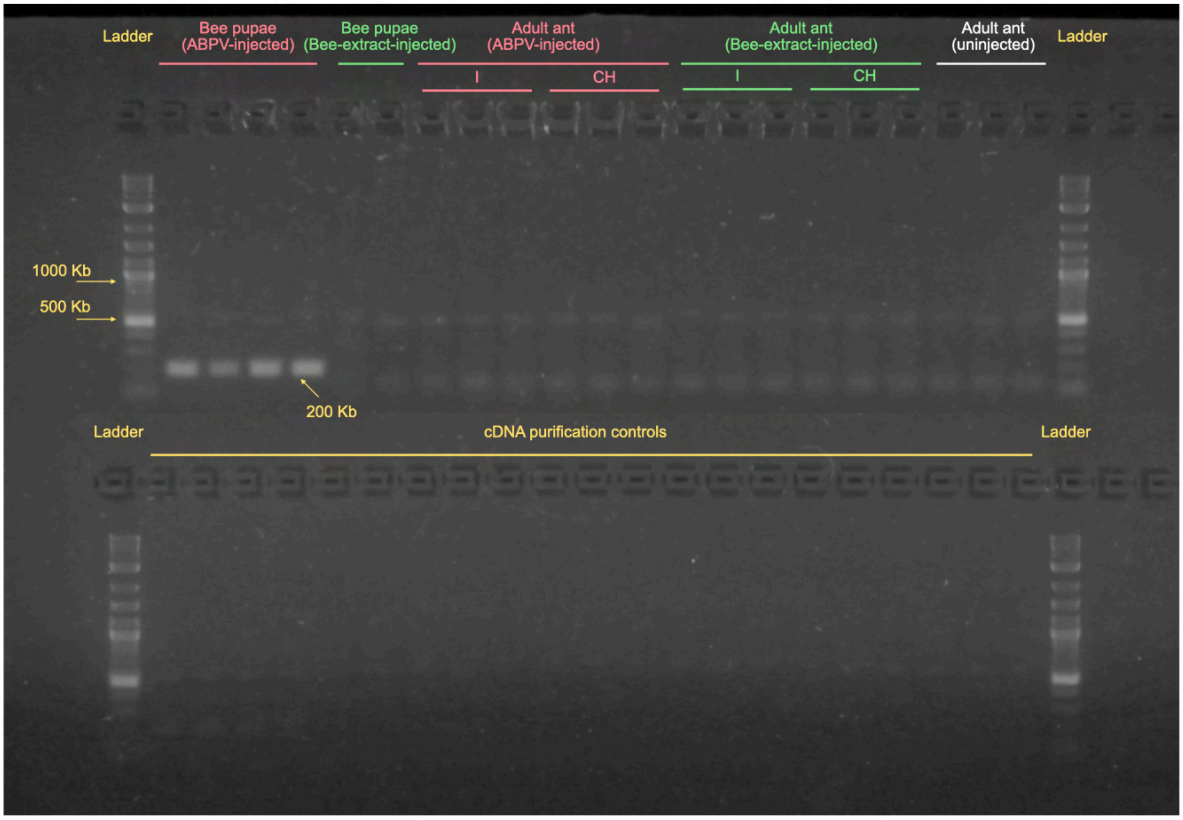


Figure 6 **Replication of ABPV in *O. biroi* 24 hrs - PI:** Red lines indicate lanes with samples containing ABPV, green lines indicate samples containing the clean bee-extract, white line indicates untreated samples, yellow lines indicate the cDNA purification controls corresponding to each well above, the 1000 kb and 500 kb bands are highlighted in the ladder for reference, the 200 kb target fragment is marked on the gel

## 3.2 *S. praecaptivus* infection response and transmission dynamics in the *O. biroi*

### 3.2.1 *S. praecaptivus* MC1 in adult ants

Mortality measurements over 14 DPI revealed a significant impact of *S. praecaptivus* on the survival of *O. biroi*. All the injected groups showed significantly lower survival compared to the uninjected control group (2K.I: ants injected with 2000 bacterial cells, 1K.I: ants injected with 1000 bacterial cells, PBS.I ants injected with PBS, ".CH" represents the corresponding cohabitating ants, 2K.I: n = 88, 1K.I: n = 96, PBS.I: n = 88, Uninjected: n = 48, 2K.CH: n = 44, 1K.CH: n = 48, PBS.CH: n = 44; AFT, 2K.I: $z$ = -5.83, $p < 0.001$, 1K.I: $z$ = -6.10, $p < 0.001$, PBS.I: $z$ = -2.29, $p = 0.02$). Log Rank tests revealed significantly higher mortalities in the bacteria-injected groups compared to PBS injection (2K, 1K: $p < 0.001$) (Figure 7 - B). No differences were observed among the cohabitating groups compared to the uninjected controls (AFT, 2K.CH: $z = 0.04$, $p = 0.97$, 1K.CH: $z = 0.47$, $p = 0.63$, PBS.I: $z = 0.38$, $p = 0.70$). These results indicate that *S. praecaptivus* significantly reduces the survival of the host ants.

Time-course monitoring of the infection status in ants revealed an increase in fluorescence in injected ants, indicating successful infection. Differences in fluorescence in *S. praecaptivus* injected ants compared to PBS-injected ants were observed starting DPI-3 (Table 4, Fig 7 - C, Fig 8 -A). Although bacteria were injected into the posterior gaster, fluorescence increased in the antenna starting from DPI-3 (S2, supplementary), indicating that the bacteria spread throughout the body within the first 72 hours post-injection. To assess potential bacterial transmission, fluorescence intensity was measured in the cohabiting ants. Since the cohabitating ants were painted on the gaster, only antennae were used for fluorescence measurement. Although the thorax and gaster also displayed a significant fluorescence increase in the injected ants ( S2, supplementary), the antenna was chosen since it displayed the strongest increase. No significant increase in fluorescence was observed in the cohabitating adults, suggesting

the absence of adult-to-adult horizontal transmission (Figure 7 - E). However, the sample size of the ants monitored regularly was small (n = 6-8 per treatment for injected groups, n = 3 - 4 per treatment for cohabitating groups). Additionally, some ants died between DPI-2 and DPI-7 (Table 4).

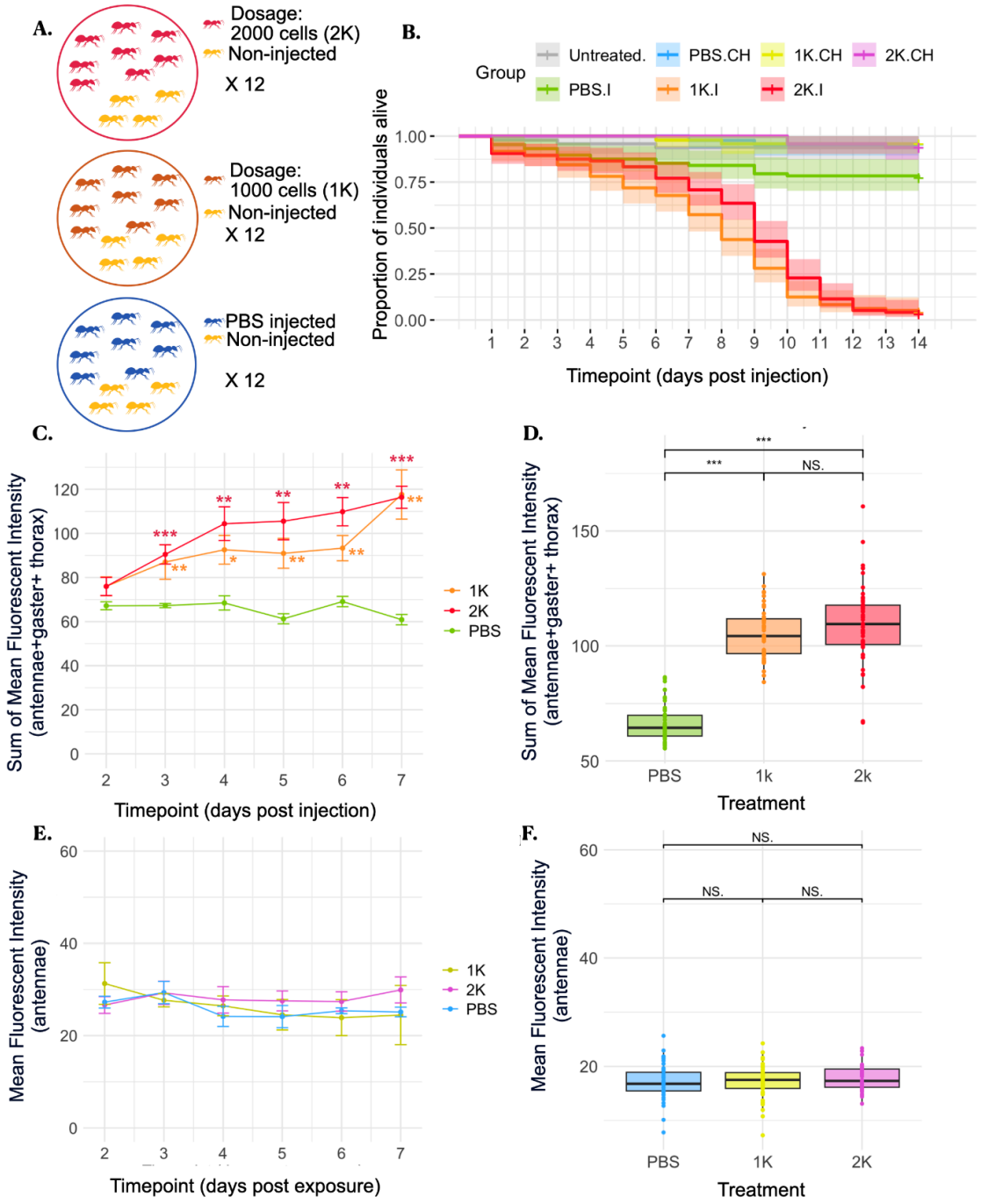

Figure 7: ***S. praecaptivus* infection and transmission dynamics in adult *O. biroi*:** (A) Experimental design (B) Kaplan-Meier survival curves, shaded regions indicate the 95% confidence interval for survival probability at each time point (n = 88 per treatment for injected ants, n= 44 per treatment for cohabitating ants, n = 44 for untreated ants) (C) Change in mean fluorescence intensity (calculated as the sum of the mean fluorescent intensity of gaster+thorax+antenna) over time in injected ants (n = 6 - 8), asterik colours indicate significance of the corresponding group compared to PBS.I, (D) Mean fluorescence intensity (calculated as C) at DPI-8 in injected ants (2K.I: n = 54, 1K.I: n = 40, PBS.I: n = 56) (E) Change in mean fluorescence intensity (antenna) over time in cohabitating ants (n= 4) (F) Mean fluorescence intensity at DPI-8 in cohabitating ants (2K.CH: n = 43, 1K.CH: n = 43, PBS.CH: n = 39); error bars in (C) and (E) represent mean ± SEM. Green, orange, and red represent ants injected with PBS, 1K, and 2K dosages, respectively; blue, yellow, and purple represent ants cohabitating ants injected with PBS, 1K, and 2K dosages, respectively. Box plots represent the median and the 25% and 75% quantile of the data, with whiskers extending to the minimum and maximum values within 1.5 times the interquartile range. '***' $p < 0.001$ '**' $p < 0.01$ '*' $p < 0.05$ 'NS' non significant

| **DPI (sample size = 2K.I, 1K.I, PBS.I)** | **Comparison** | ***p*-value** | **DPI (sample size = 2K.I, 1K.I, PBS.I)** | **Comparison** | ***p*-value** |
|---|---|---|---|---|---|
| 2 (n = 6, 8, 7) | 1K vs 2K | 1 | 5 (n = 6, 6, 7) | 1K vs 2K | 0.54 |
| | 1K vs PBS | 0.06 | | 1K vs PBS | < 0.01 ** |
| | 2K vs PBS | 0.30 | | 2K vs PBS | < 0.01 ** |
| 3 (n = 8, 7, 7) | 1K vs 2K | 0.36 | 6 (n = 6, 6, 7) | 1K vs 2K | 0.224 |
| | 1K vs PBS | < 0.001 ** | | 1K vs PBS | < 0.001 ** |
| | 2K vs PBS | < 0.001 *** | | 2K vs PBS | < 0.001 ** |
| 4 (n = 6, 7, 7) | 1K vs 2K | 0.68 | 7 (n = 6, 6, 7) | 1K vs 2K | 1 |
| | 1K vs PBS | 0.01 * | | 1K vs PBS | < 0.01 ** |

| | | | | | |
|---|---|---|---|---|---|
| | 2K vs PBS | <0.01 ** | | 2K vs PBS | < 0.01 ** |

Table 4. **Time progression of *S. praecaptivus* infection in *O. biroi***: Statistics of change in fluorescent intensity over time in injected ants '***' $p < 0.001$ '**' $p < 0.01$ '*' $p < 0.05$

In order to confirm the findings and assess the frequency at which *S. praecaptivus* can infect the host ant, all ants alive at DPI-8 were assessed for fluorescence to further confirm the observed results. A difference in fluorescence was observed across treatment groups (2K.I: n = 54, 1K.I: n = 40, PBS.I: n = 56, Kruskal Wallis Test, $\chi^2 = 101.92$, df = 2, $p < 0.001$, Fig 7 - D). An increase in fluorescence was observed in ants treated with 1K and 2K bacterial cells compared to PBS-injected controls (Dunn's test, 2K-1K, $p = 1$; PBS-1K, $p < 0.001$; PBS-2K, $p < 0.001$). No differences were observed between the two dosages, indicating that 1000 bacterial cells are sufficient to establish infection. At DPI-8, 100% of surviving ants receiving a dosage of 1000 cells and 96.3% of ants receiving a dosage of 2000 cells developed the infection, confirming that *S. praecaptivus* can effectively infect and sustain until death in *O.biori*. The two ants that did not display fluorescence are presumed to have resulted from injection error.

Fluorescence intensity in cohabitating revealed no transmission among colony mates. No differences were observed across treatment groups (2K.CH: n = 43, 1K.CH: n = 43, PBS.CH: n = 39, ANOVA $F(2, 124)$, $p = 0.5$, Figure 7 - E, F). This confirmed the absence of adult-to-adult transmission of *S. praecaptivus* in *O. biroi*.

We found a lower number of eggs laid in the infected colonies compared to the control colonies (2K-1K, $p = 1$; PBS-1K, $p = 0.01$; PBS-2K, $p = 0.01$; Figure 8 - B), indicating that *S. praecaptivus* infection reduces host fecundity. However, since the cohabitating ants also contributed to egg-laying in the infected colonies, further experiments with colonies consisting of only infected ants are required to accurately determine the number of eggs laid by the infected ants.

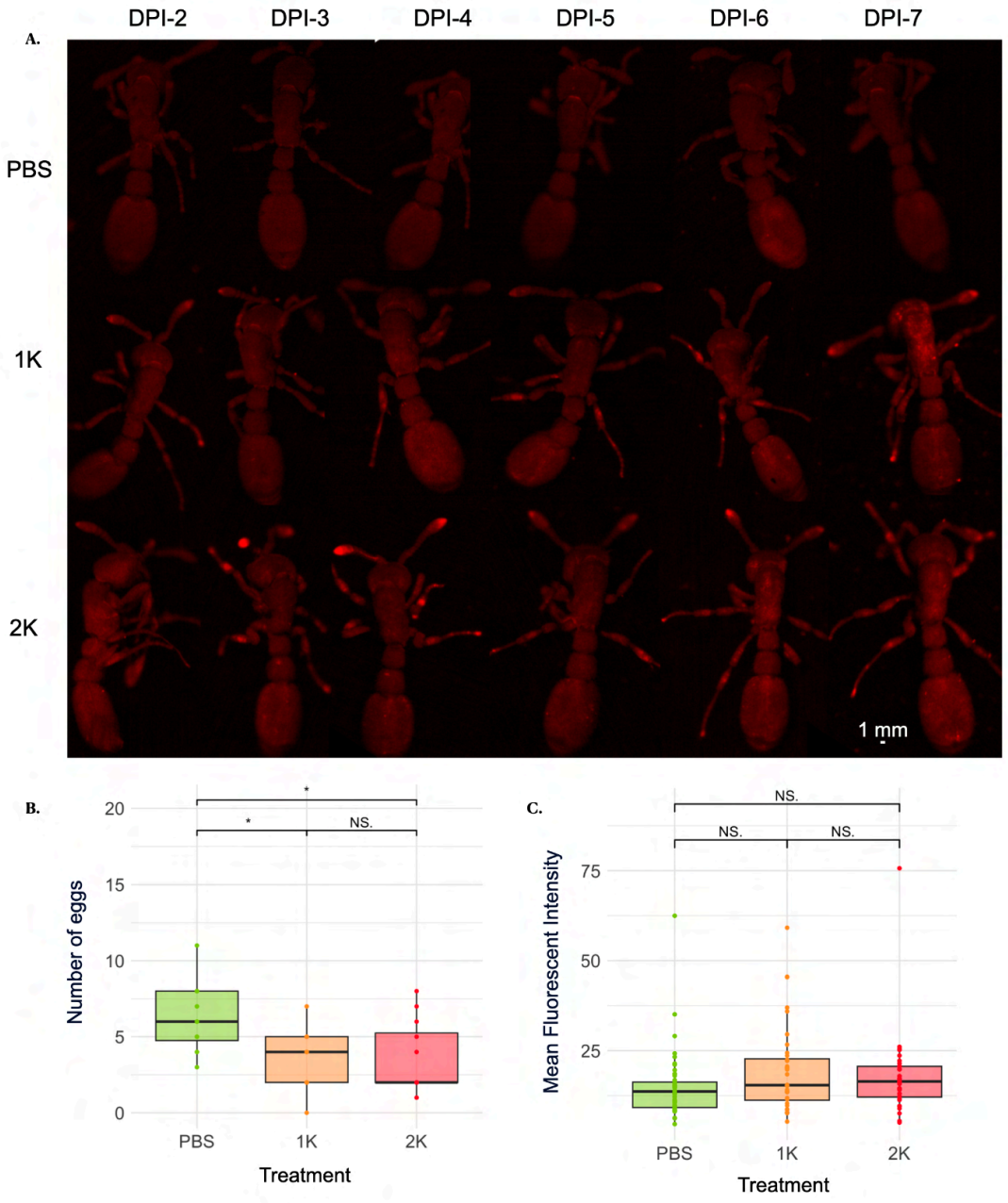


Figure 8 ***S. praecaptivus* infection progression in adult *O. biroi* and impact on egg laying and horizontal transmission** (A) Progression of infection in adult ants over time, adults picked randomly from the additional replicate for regular monitoring (B) Number of eggs laid per plate (n = 12 plates per treatment, 8 injected and four cohabitating adults per plate) (C) Mean fluorescence intensity in eggs collected from the plates at DPI-7. Green, orange, and red represent ants injected with PBS, 1K, and 2K dosages of *S. praecaptivus*, respectively. Box plots represent the median and the 25%

and 75% quantile of the data, with whiskers extending to the minimum and maximum values within 1.5 times the interquartile range. '***' $p < 0.001$ '**' $p < 0.01$ '*' $p < 0.05$ 'NS' non - significant

In order to assess the vertical transfer of bacteria, fluorescence intensity measurements were conducted on eggs laid by ants in all treatment groups. No significant differences were observed between the three treatment groups (Kruskal Wallis Test, $\chi^2 = 5.00$, df = 2, $p = 0.08$; Figure 8 - C). This could indicate absence of vertical transmission or the absence of egg-laying by the infected adults. Furthermore, the lack of fluorescence in the eggs, despite prolonged exposure to infected individuals within the colony, suggests effective mechanisms preventing pathogen adult-to-egg horizontal transmission in infected colonies.

Given the infectivity of the bacteria and its effects on the host survival and fecundity, the melanization of all injected ants across all treatment groups was measured at DPI-8. Melanization was lower in the infected groups (2K.I: n = 54, 1K.I: n = 40, PBS.I: n = 72; ANOVA, $F(1, 163) = 6.10$, $p < 0.01$). No difference was observed between the two injected groups (Tukey's post hoc, 2K-1K, $p = 0.98$; PBS-1K, $p = 0.01$; PBS-2K, $p = 0.01$, Figure 9).

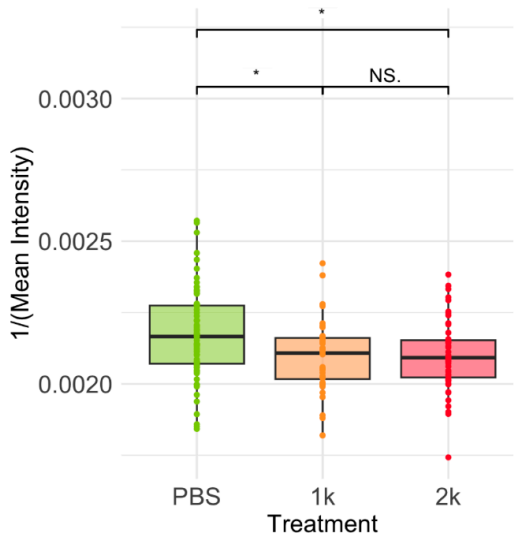


Figure 9: ***S. praecaptivus* infection melanization response in adult *O. biroi*:** Whole body melanization (gaster + thorax + head) in injected ants at DPI-8. Green, orange, and red represent ants injected with PBS, 1K, and 2K dosages, respectively. Box plots represent the median and the 25% and 75% quantile of the data, with whiskers extending to the minimum and maximum values within 1.5 times the interquartile range.

‘***’ $p < 0.001$ ‘**’ $p < 0.01$ ‘*’ $p < 0.05$ ‘NS’ non-significant (refer to S4, supplementary for area specific melanization)

### 3.2.3 FISH in *S. praecaptivus* infected adult ants

FISH of *S. praecaptivus* injected ants (2K.I) at 9 DPI revealed the presence of the bacteria across all observed body parts. *S. praecaptivus* was present in the fat bodies of the gaster, in the brain, and at the tip of the antennae (Figure 10). *S. praecaptivus* clusters were observed in the muscle cells in the gaster as well as the head (thin arrows, Figure 10). Although injections were made at the tip of the gaster, *S. praecaptivus* was found to be nearly equally distributed across the gaster and the head. This suggests that *S. praecaptivus* might be present in the insect hemolymph. In addition, inside the gaster or the brain, the bacteria were present across different areas suggesting that the bacteria do not localize in site specific manner in the host. Within the gaster, *S. praecaptivus* was also localized in the cell body of the neurons of the abdominal ganglia (red arrow Figure 12 A). Clusters of *Sodalis* were detected within the ovarian tissue (Figure 11- B, C, D), suggesting a possibility of vertical transmission. Some regions of the ant, like the outer cuticle, were autofluorescent across all samples (Figure 10, 11). Some cell boundaries of the fat bodies and muscle cells displayed mild autofluorescence. However, these regions were distinctly different from the comparatively higher fluorescence intensity of the bacterial signal. In all the cases, the presence of *S. praecaptivus* was confirmed by looking into the overlap between the *Sodalis*-specific probe and the general eubacterial probe and comparing with the controls. Control groups, consisting of both uninjected ants and PBS-injected ants, showed no presence of *Sodalis*. Since a general *Sodalis* probe was used for hybridization, this confirmed that *Sodalis* is not naturally present in *O. biroi*.

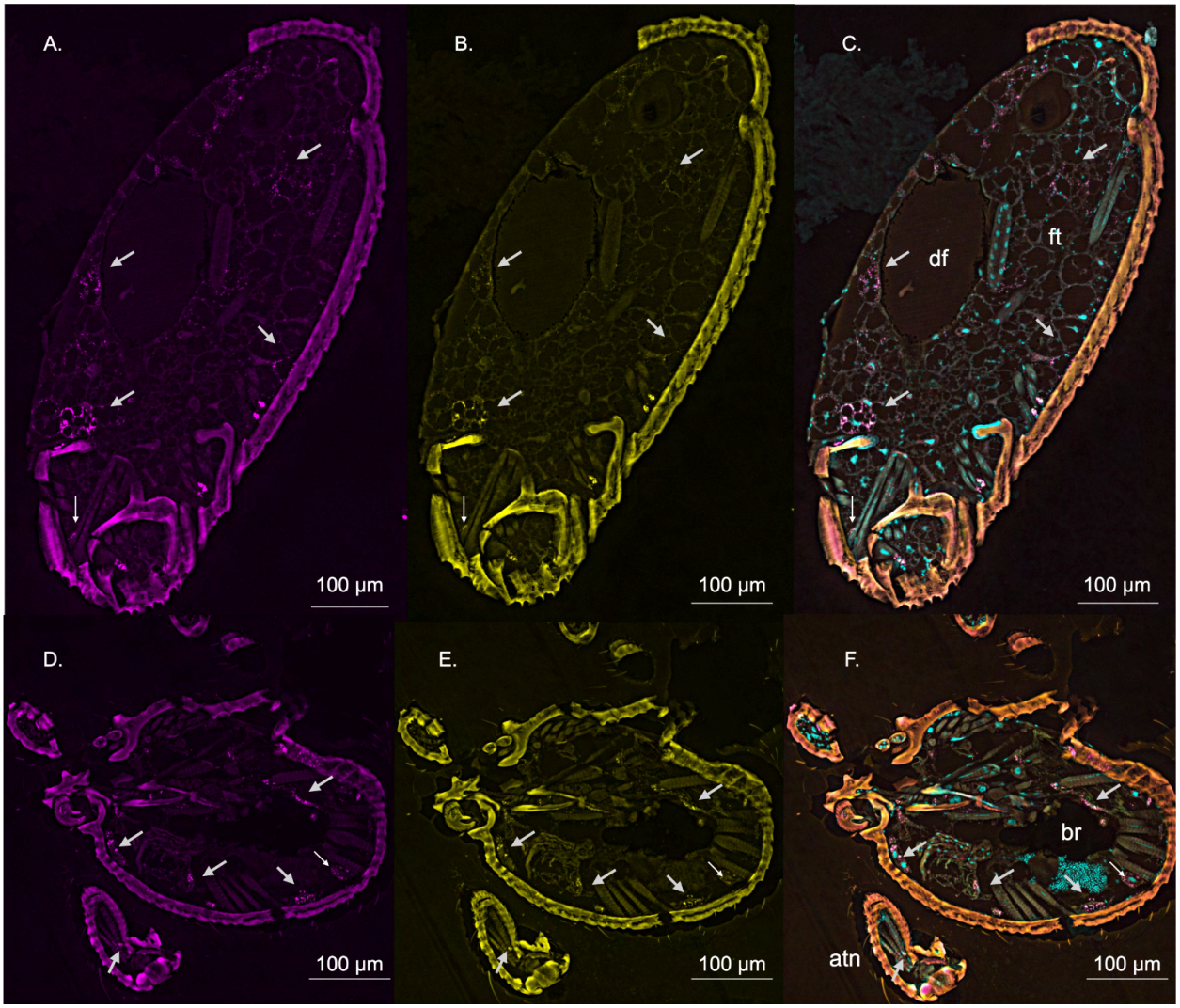


Figure 10: ***S. praecaptivus* localization in the gaster and head of *O. biroi*.** Localization of *Sodalis* (magenta), all eubacteria (yellow) in the gaster (A, B, C) and head (D, E, F) of adult *O. biroi* at DPI-9 (C, F) represent the colocalization of the *Sodalis* and eubacteria probe counterstained with DAPI. Thick arrows represent bacterial clusters in the fat bodies, and thin arrows represent bacterial clusters in the muscle cells. Br: brain, atn: antenna, df: Dufour gland, ft: fat body

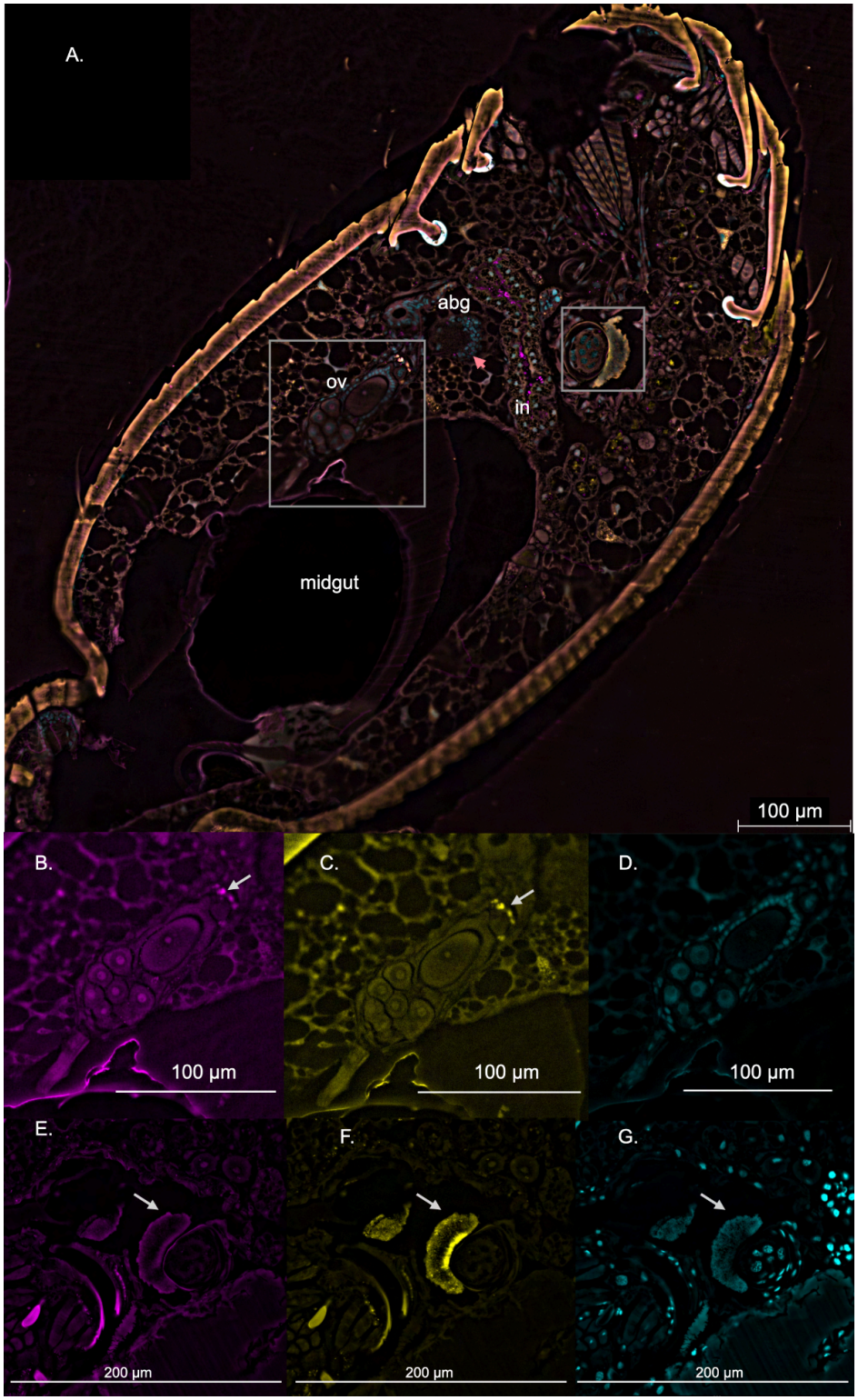


Figure 11 ***S. praecaptivus* localization in ovary and bean-shaped organ in the gaster of injected adult *O. biroi***: (A) gaster showing overlap of *S. praecaptivus* (magenta), all eubacteria (yellow), DAPI (cyan); abg - abdominal ganglia, in - intestine,

ov - ovary; red arrow indicates bacteria cluster in abg; squares represent the areas of interest focussed in the subsequent panels (B, C, D) Ovary of an adult injected ant showing localization of *S. praecaptivus,* arrows indicate bacteria cluster (E, F, G) bean-shaped structure observed in the gaster, arrows indicate the structure, square

A highly fluorescent region in the gaster was observed at the posterior end of the gaster (Figure 11 - E, F, G). This structure appeared bean-shaped and was present in proximity to a circular, tube-like structure with prominent nuclei. This structure had a dense labeling for eubacteria compared to specific *S. praecaptivus*. This suggested the presence of other bacteria in this region. A similar structure was also observed in the uninjected ant, where only eubacteria was present (Figure 12). In the uninjected ant, too, this structure was located towards the posterior gaster and is visible at a similar distance from the abdominal ganglia (Figure 11 - A, 12 - A). This suggests the presence of non-*Sodalis* eubacteria in the ants at a specific site in the gaster. However, further characterization and imaging of a larger number of samples is required to confirm these findings.

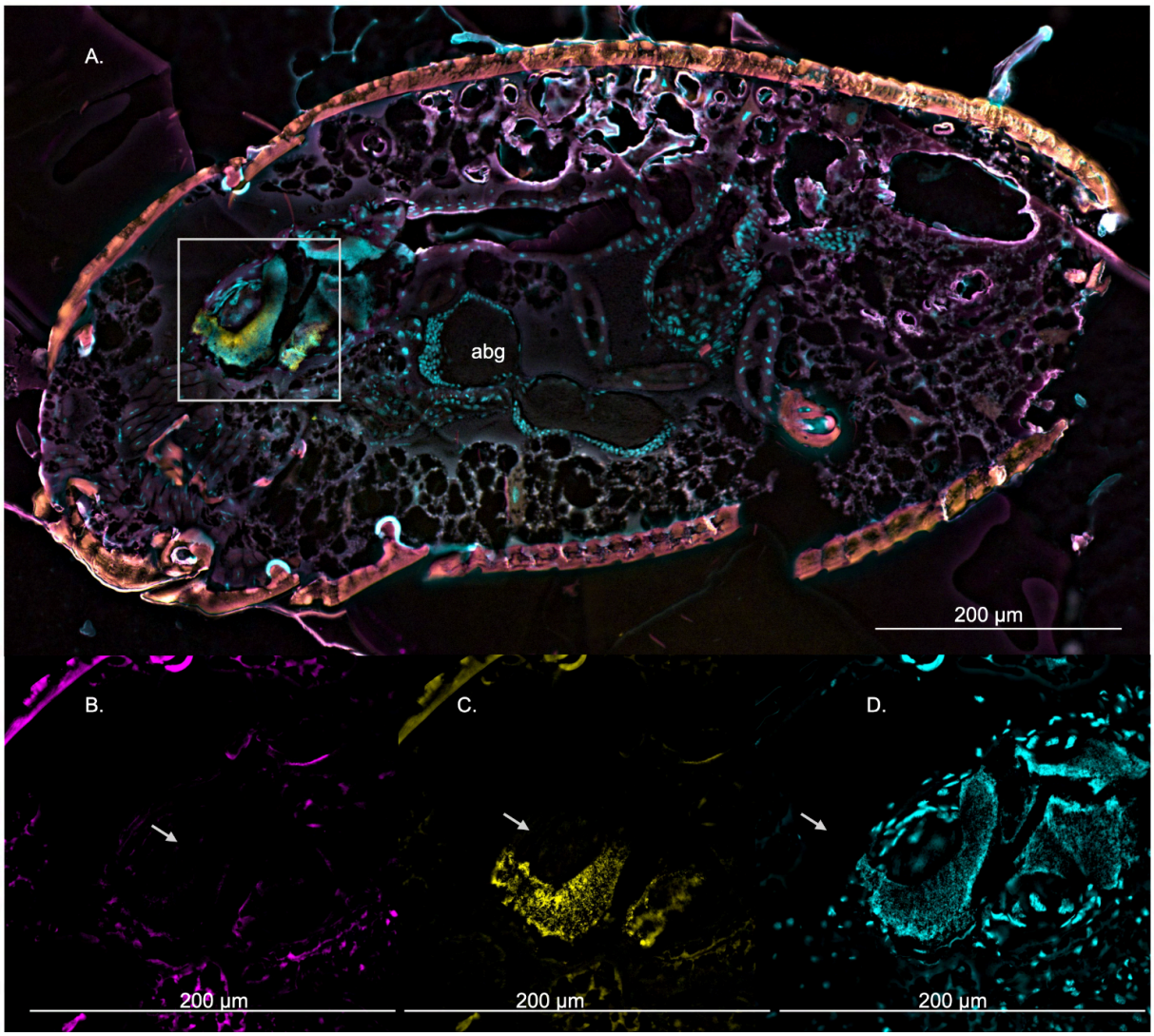


Figure 12. **Eubacteria localization in uninjected *O. biroi* adults**: (A) Localization of *S. praecaptivus* (magenta), eubacteria (yellow) in an uninjected *O. biroi* adult counterstained with DAPI (cyan), square marks the region magnified in subsequent images, the abdominal ganglia (abg) is marked (B, C, D) Bean shaped structure containing eubacteria at higher magnification, arrows indicate this structure

### 3.2.3 *S. praecaptivus* MC1 infection in pupae

*S. praecaptivus* injected pupae showed higher mortality compared to the uninjected control group (25cpn.l pupae injected with 25 cells/nL, 10cpn.l pupae injected with 10

cells/nL, PBS.I pupae injected with PBS; 25cpn.I: n = 36, 10cpn.I: n = 36, PBS.I: n = 36, Uninjected: n = 12; AFT, 25cpn.I: $z$ = -6.04, $p$ < 0.001, 10cpn.I: $z$ = -5.81, $p$ < 0.001, PBS.I: $z$ = -1.80, $p$ = 0.72, Figure 13 - B). No differences were observed among the adults cohabitating infected pupae compared to adults cohabitating uninjected pupae (25cpn.CH: adults cohabitating 25cpn.I, 10cpn.CH: adults cohabitating 10cpn.I, PBS.CH: adults cohabitating PBS.I, 25cpn.CH: n = 48, 10cpn.I: n = 48, PBS.I: n = 48, Uninjected: n = 16; AFT, 25cpn.I: $z$ = 1.3, $p$ = 0.195, 10cpn.I: $z$ = 0.21, $p$ =0.07, PBS.I: $z$ = 1.24, $p$ = 0.21, Figure 13 - B). These results indicate that *S. praecaptivus* significantly reduces the survival of *O. biroi* pupae but does not impact the survival of cohabitating adults.

Pupae injected with *S. praecaptivus* showed an increase in fluorescence from DPI-2 (n = 4 - 6 per treatment per timepoint; Two way ANOVA main effect, Treatment: $F(2, 33)$ = 28.81, $p$ < 0.001, Timepoints: $F(1, 33)$ = 112.92, $p$ < 0.001; interaction $F(2, 33)$ = 35.15, $p$ < 0.001, Figure 13 - C). No differences were observed between the fluorescence intensity in the two groups of injected pupae, suggesting 10 cells/nL was sufficient to establish infection (Tukery's post hoc: DPI-2: 25cpn -10cpn, $p$ = 0.76; PBS-10cpn, $p$ = 0.07; PBS-25cpn, $p$ = 0.01; DPI-3: 25cpn - 10cpn, $p$ = 0.96; PBS-1K, $p$ < 0.001; PBS-25cpn, $p$ < 0.001).

To validate the initial observations and increase the sample size, all live pupae from all the replicates were imaged at DPI-4. Pupae injected with 10cpn and 25cpn of bacteria had higher fluorescence compared to PBS-injected pupae (25cpn.CH: n = 23, 10cpn.I: n = 19, PBS.I: n = 23; Kruskal Wallis Test, $\chi^2$ = 43.29, df = 2, $p$< 0.001, Dunn's test: 25cpn - 10cpn, $p$ = 0.91; PBS-1K, $p$ < 0.001; PBS-25cpn, $p$ < 0.001) (Figure 14 - D). These results further confirmed that *S. praecaptivus* successfully infects and propagates in the *O. biroi* pupae. Although the bacteria were injected into the gaster, whole-body localization of the bacteria was observed starting DPI-2 (Figure 14 - A). The early development of infection compared to the injected adults could be because the bacteria propagate faster in pupae compared to the adults. It could also be due to the

ease of detecting the fluorescence in the pupae compared to the adults with a highly melanized cuticle.

Since ant pupae produce pupal fluid that is consumed by both adults and larvae (Snir et al. 2022), bacteria could potentially transmit from pupae to adults. To assess this, fluorescence intensity was measured in adult ants cohabitating with injected pupae 16 days post-initial exposure to pupae. Given that infection in adults developed over 8 days post-injection in adults (Section 3.2.1), this time point was chosen to allow sufficient time for the bacteria to grow within the adult host in case of an event of transmission. However, no significant differences in fluorescence intensity were observed between adults cohabitating with either bacteria-infected or control pupae, suggesting the absence of pupal-to-adult transmission (25cpn.CH: n = 38, 10cpn.CH: n = 44, PBS.CH: n = 42 Kruskal Wallis Test, $\chi^2 = 3.88$, df = 2, $p = 0.14$; Figure 14 - E) (for area wise change on fluorescent intensity refer to S5, supplementary). *O. biroi* colonies containing adults and pupae also contain eggs laid by the adults. Eggs present in all experimental plates were collected at DPI-16, and their fluorescent intensity was measured. No significant differences in fluorescence intensity were detected between eggs or larvae collected from bacteria-infected and control plates (25cpn colonies: n = 14, 10cpn colonies: n = 18, PBS colonies: n = 24, Kruskal Wallis Test, $\chi^2 = 0.6$, df = 2, $p = 0.73$ Figure: 15 -B), indicating no horizontal transfer from infected pupae to eggs of the following generation.

At DPI-4, when the infection was well established, increased melanization was observed in infected pupae (Fig 3.2.6 - C) compared to the PBS-injected controls (25cpn - 10cpn, $p = 0.91$; PBS-1K, $p < 0.001$; PBS-25cpn, $p < 0.001$) (Fig 3.2.6 - D). Small circular sports of intense melanization were observed at various parts of the body including the spot of injection. This could be due to nodule formulation.

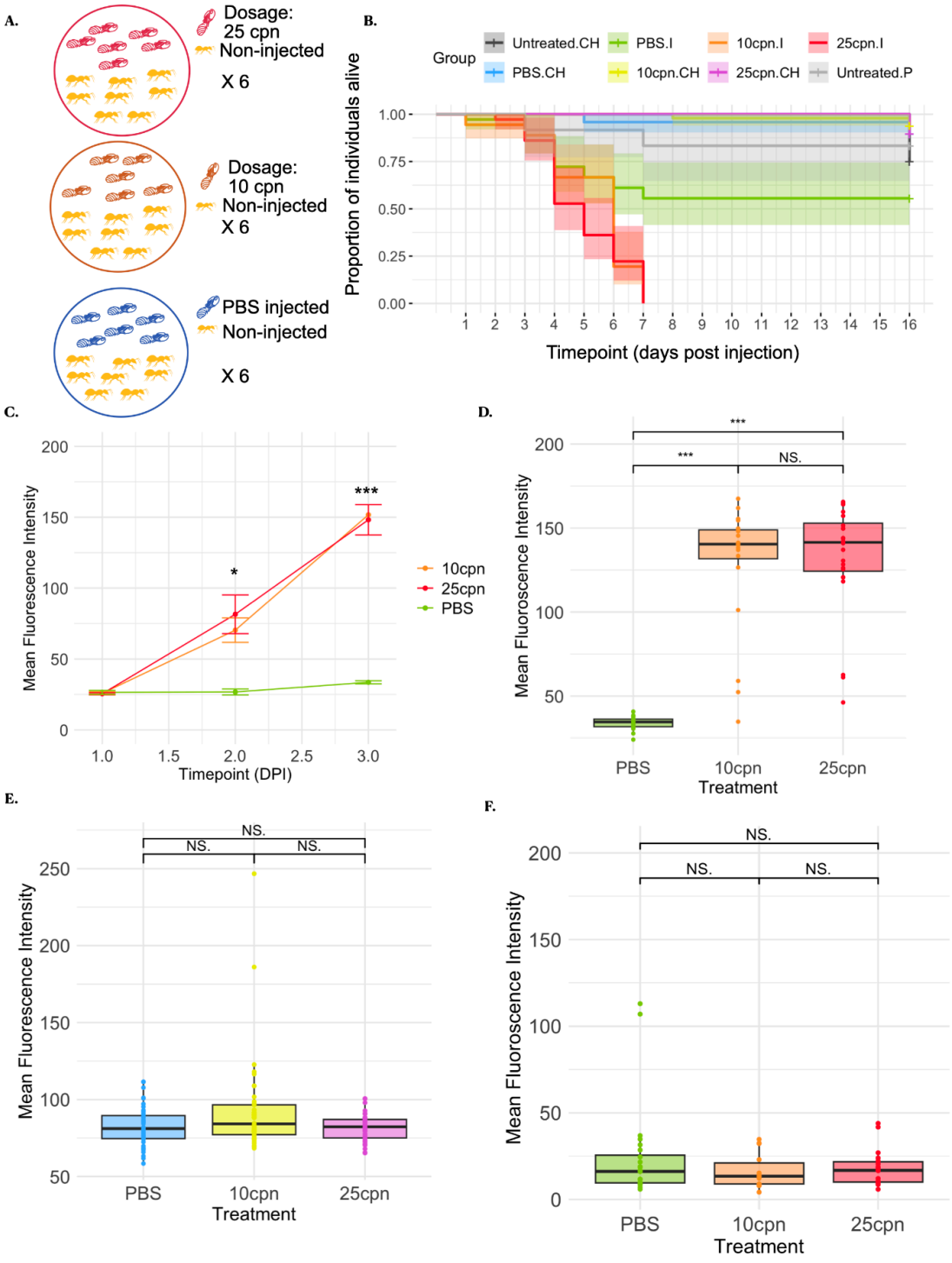


Figure 13 ***S. praecaptivus* infection and transmission dynamics in *O. biroi* pupae:** (A) Experimental design (B) Kaplan-Meier survival curves, shaded regions indicate the 95% confidence interval for survival probability at each time point (n = 36 per treatment

for injected ants, n= 48 per treatment for cohabitating ants, n = 12 for untreated pupae, n = 16 for untreated cohabitating adults) (C) Change in mean fluorescence intensity (gaster+thorax+antenna) over time in injected ants (n = 6 per treatment); error bars represent mean ± SEM (D) Mean fluorescence intensity at DPI-4 in injected pupae (25cpn.CH: n = 23, 10cpn.I: n = 19, PBS.I: n = 23) (E) Mean fluorescence intensity at DPI-16 in cohabitating ants (25cpn.CH: n = 38, 10cpn.CH: n = 44, PBS.CH: n = 42); Green, orange, and red represent pupae injected with PBS, 10cpn, and 25cpn dosages, respectively; blue, yellow, and purple represent ants cohabitating ants injected with PBS, 10cpn, and 25cpn dosages, respectively (F) Mean fluorescence intensity at DPI-16 of eggs collected from all the replicates; '***' $p < 0.001$ '**' $p < 0.01$ '*' $p < 0.05$ 'NS' non significant

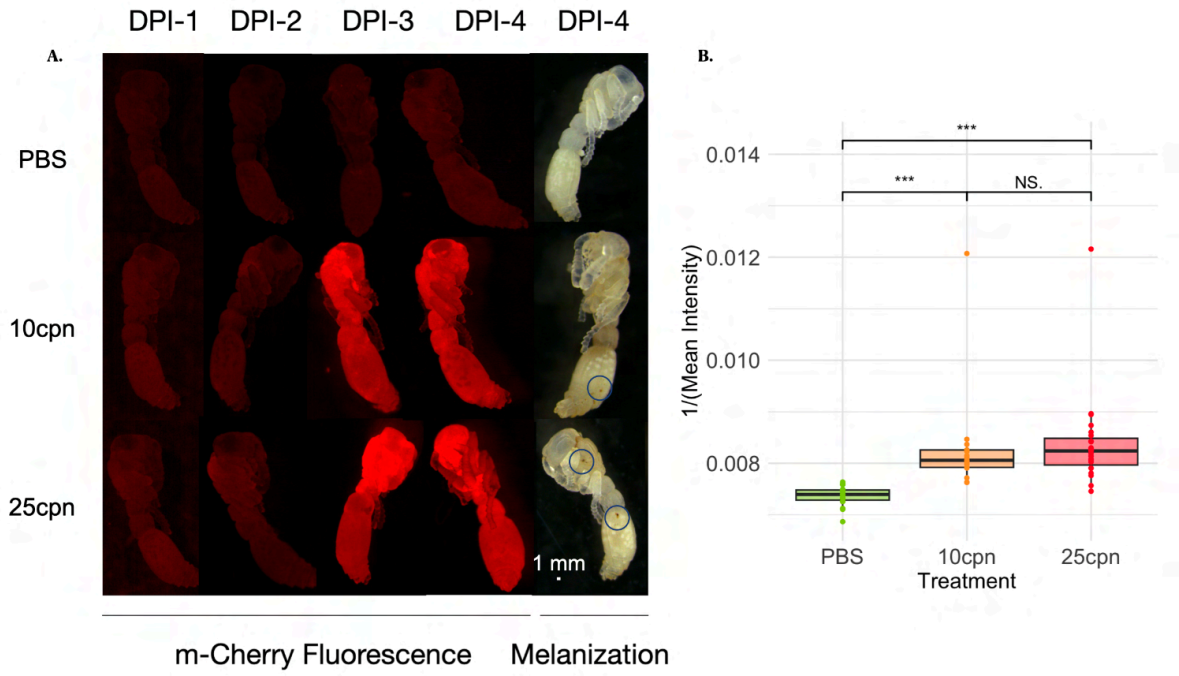


Figure 14 **Progression of *S. praecaptivus* infection progression *O. biroi* pupae and melanization response:** (A) Progression of infection in the pupae over 4 days post-injection; Melanization in pupae of different treatment groups (B) Quantification of melanization in pupae of different treatment groups at DPI-4 (25cpn.CH: n = 23, 10cpn.I: n = 19, PBS.I: n = 23). Circles on the melanization panel represents melanin spots. Green, orange, and red represent pupae injected with PBS, 10cpn, and 25cpn dosages of *S. praecaptivus* '***' $p < 0.001$ '**' $p < 0.01$ '*' $p < 0.05$ 'NS' nonsignificant

### 3.2.4 *S. praecaptivus* MC1 infection in eggs

To investigate bacterial transmission dynamics across various developmental stages, eggs laid over 48 hours were injected. Injected eggs began hatching 7–8 days post-injection, with an overall hatching rate of 8.30% (Table 5). This is comparable to previously observed hatching rates of 1.8% and 7.8% in low and high pressures, respectively (Trible et al. 2017). Despite maintaining the same bacterial concentrations and environmental conditions, the hatching rate varied considerably between the different batches of injected ants. Figure 15 (a - d) shows the progression of the infection within the developing embryo (images taken from randomly picked eggs on each day). By DPI-3, a distinct region of high-intensity fluorescence was observed at the injection site (Figure 15 a). Fluorescent imaging within 24 hrs of hatching revealed sodalis localization of the bacteria in larvae, with the most intense fluorescence detected in the gut (Figure 15 e, f). A substantial proportion of successfully hatched larvae (60.71%) retained the bacteria, indicating efficient egg-to-larva transmission (Table 5). Additionally, gut peristalsis was observed under the microscope, confirming that the larvae were alive within 24 hrs of hatching.

Since larvae in social insects like *O. biroi* require parental care to successfully develop into adults, hatched larvae were transferred to plates containing young callows for further growth. Fluorescent larvae were initially visible within the larval cluster in the rearing units (Figure 15 f), indicating that adult ants actively carried them to their nesting site. However, the infected larvae disappeared from the clusters or lost fluorescence 2 - 3 days post-hatching. Several modifications were implemented to the rearing units in an attempt to prevent this outcome. First, only early-stage callows were used as workers. Additionally, workers from different genotypes were used to account for potential behavioral differences in brood care (Jud et al. 2022). Since early-stage larvae cohabit with pupae and consume pupal fluid, pupae were introduced into the rearing units. Furthermore, the ratio of infected to control larvae within a rearing unit was varied, with some units containing a majority of infected individuals and others a majority of controls. Rearing units consisting of only infected larvae were also set up. Despite these modifications, in all rearing units, larvae consistently disappeared within 2–3 days post-hatching. Further experiments are required to understand the causes for this

occurrence and to explore the feasibility of achieving an infected adult through egg injections.

| | Uninjected control | | | Sodalis injected | | | | |
|---|---|---|---|---|---|---|---|---|
| **Batch** | **Number of eggs** | **Number of eggs hatched** | **Proportion of eggs hatched** | **Number of eggs injected** | **Number of eggs hatched** | **Proportion of eggs hatched** | **Number of fluorescent larvae** | **Proportion of fluorescent larvae** |
| **1** | 90 | 31 | 34.44% | 300 | 28 | 9.33% | 14 | 50.00% |
| **2** | 150 | 64 | 42.67% | 279 | 37 | 13.26% | 31 | 83.78% |
| **3** | Same as Batch 2 | | | 250 | 7 | 2.80% | 6 | 85.71% |
| **4** | 80 | 30 | 37.50% | 257 | 15 | 5.84% | 13 | 86.67% |
| **5** | 125 | 58 | 46.40% | 308 | 58 | 18.83% | 21 | 36.21% |
| **6** | 151 | 34 | 22.52% | 433 | 22 | 5.08% | 19 | 86.36% |
| **7** | Same as Batch 6 | | | 308 | 7 | 2.27% | 6 | 85.71% |
| **8** | 56 | 24 | 42.86% | 227 | 22 | 9.69% | 9 | 40.91% |
| **Total** | 652 | 241 | 36.96% | 2362 | 196 | 8.30% | 119 | 60.71% |

Table 5. **Hatching success in eggs injected with *S. praecaptivus***: Number of eggs hatched in control and injected groups within 14 DPI. Proportion of eggs hatched is calculated as {(No. of eggs hatched)/(total number under observation)}*100%; Proportion of fluorescent eggs calculated as {(No. of fluorescent larvae)/(No. of injected eggs hatched)}*100%; since batches 2, 3 and 6, 7 were conducted on consecutive days, the same set of conditional controls was used

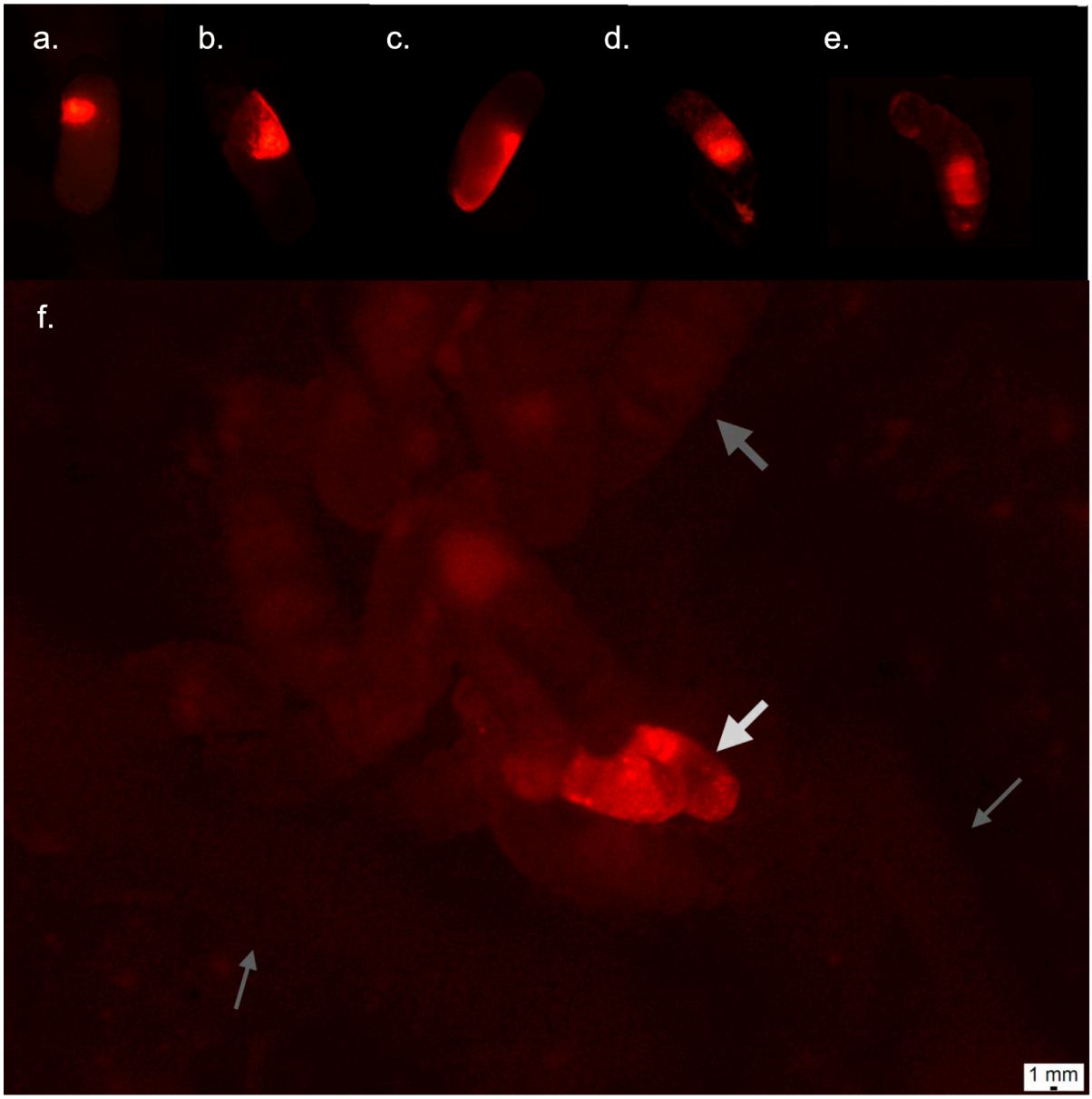


Figure 15 ***S. praecaptivus* infection and transmission dynamics in *O. biroi* egg:** a, b, c, d shows infection spread in the egg; d, e show infected larvae that hatched after *S. praecaptivus* injection; f shows infected larvae within a larval cluster one day after being transferred to a rearing unit, broad white arrow indicate the infected larvae, broad grey arrow indicate cohabitating non-injected larvae, thin grey arrows indicate adults surrounding the larval cluster (out of focus)

# Discussion

In this thesis, we have investigated the impact of two novel putative pathogens: ABPV and *S. praecaptivus,* in *O. biroi.* Both of these have never been reported in *O. biroi* but have the ability to infect their non-natural hosts (Schläppi et al. 2020; Su et al. 2022). Our results indicate that both pathogens have distinct capabilities of infecting and replicating in the host. While *S. praecaptivus* successfully spreads in the whole body of the host, ABPV fails to establish infection. Consequently, the impacts on host survival and immune response is also different. However, in both cases, no transmission is observed.

ABPV did not replicate within *O. biroi* and did not induce in *Dcr-2* expression. This lack of immune response could be attributed to the absence of viral replication in the host. *Dcr-2* is primarily responsible for targeting dsRNA for degradation (Flenniken and Andino 2013), which in the case of ABPV, is a replication intermediate. In the absence of viral replication, the *Dcr-2*-mediated immune response may not have been upregulated. Previous studies on field samples of multiple ant species have shown the absence of *Dcr-2* response associated with other honeybee viruses like DWV, KBV, BQCV (Lester et al. 2019; Viljakainen et al. 2023). However, very little is known about immune responses to ABPV. Our results confirm that the *Dcr-2*-based RNAi pathway is not activated as an antiviral response to ABPV in *O. biroi.* This is consistent with the findings in honeybees, the natural hosts for ABPV, where no *Dcr-2* upregulation was observed post-infection (Azzami et al. 2012). Future experiments are required to explore other immune pathways that might be upregulated in response to ABPV infection in ants.

A possible reason for the lack of viral infection could be the mode of administration used in our experiments. Previous studies show that foodborne transmission of ABPV is possible in ants and bumblebees (Schläppi et al. 2020; Tehel et al. 2022). However, foodborne transmissions require higher viral titers than the maximum titres at hand in the lab stocks used for the current experiments. Future experiments need to be

conducted using feeding to confirm foodborne ABPV infection in *O. biroi.* The virus's inability to establish infection in a non-native host could also be due to the absence of host-specific machinery necessary for viral replication. This could be due to host-pathogen co-evolution and ecological barriers to cross-species transmission (Webby et al. 2004). Recent studies have shown that ant viruses found in field samples are mostly species-specific, with only a few viruses found across different species or geographic regions (Viljakainen et al. 2023). Although honeybee viruses are commonly associated with ants (Baty et al. 2020), many of them might be found as contaminants on the surface (Viljakainen et al. 2023). Such species specificity of ant-viruses also provides a plausible explanation for the inability of ABPV to replicate within the injected ants.

In contrast to the virus, *S. praecaptivus* was able to successfully infect *O. biroi*, leading to a significant decrease in lifespan and reduced fecundity—both of which are detrimental to colony fitness. Our experiments show that *S. praecaptivus* could successfully establish infection across all the life stages: egg, larvae, pupae, and adult. Despite the virulance of *S. praecaptivus*, no horizontal or vertical transmission was observed. Vertical transmission cannot be dismissed since our experiment to test the egg-laying of infected ants was performed in the presence on uninfected cohabitating adults. The cohabitating adults might have dominated egg-laying in infected colonies or cannibalized the eggs laid by infected colony mates (Bizzell and Pull 2024). Future experiments are required to test the egg laying in colonies consisting of only infected individuals to confirm the absence of vertical transmission.

FISH in adult ants shows that *S. praecaptivus* is present across different regions of the the body in the injected adults. Bacteria localization is visible in the fat bodies of the gaster, in the brain, and at the tip of the antenna. Bacterial clusters were also observed in the ovary, suggesting a potential for vertical transmission. A bean-shaped structure possessing a high density of eubacteria was also identified in the gaster in both injected and non-injected ants. *S. praecaptivus* was present inside this bean-shaped structure in the infected ants but not in the uninjected control. These findings suggest this structure could be a potential bacteriome. However, the current sample size is not sufficient to

confirm these findings. Gut microbiota profiling and micro-CT scan (Computer tomography scan) could help in understanding the contents of the structure and its positions in the gaster, respectively.

In response to infection, a developmental stage-specific melanization response was observed in *S. praecaptivus* infected adults and pupae. Adult ants exhibited decreased cuticular melanization, consistent with findings of grain weevils infected with *S. praecaptivus* (Su et al. 2022). In the grain weevils, no effect on melanization was observed when a tyrosine-overproducing strain of *S. praecaptivus* was used for infection, suggesting that decreased melanization could be due to the pathogen depleting host tyrosine resources, leading to insufficient tyrosin for cuticular melanization. However, how this might be related to the immune melanization response is unknown. In contrast, since ant pupae do not have sclerotized cuticle, the increase in melanization observed could potentially be an indicator of the humoral melanization response. Pupae also displayed nodule-like structures in different locations of the body, which is an additional indicator of a melanin-based immune response (Smith et al. 2022). These combined results raise the possibility that the combined tyrosine pool of both host and pathogen is differentially allocated depending on the developmental stage, with distinct physiological trade-offs between immune defense and cuticular development.

Egg injections with *S. praecaptivus* resulted in larvae containing the bacteria. However, infected larvae disappeared from the rearing units 2-3 days after hatching. This could be due to multiple reasons: (a) the larvae died (b) the workers detected chemical ‘sickness cues’ from the infected larvae and discarded or cannibalized (after or before death) them as a method of colony disinfection (Pull et al. 2018), (c) the larvae might have cleared the infection Since larvae disappeared from colonies consisting of only infected larvae, it is unlikely that bacteria were eliminated by the larval immune system. Behavioral recordings of rearing units consisting of infected larvae can shed light on the underlying mechanism of the disappearance of infected larvae.

Future transcriptomic analysis of *Sodalis*-infected ants investigating the changes in immune gene expression and tyrosine regulation pathways can provide information about how infection alters host biology. Currently, not much is known about how various behaviors such as self-grooming, allogrooming, and social isolation change with infection progression. The infection development over a period of 14 days makes the *O. biroi - S. praecaptivus* system a powerful tool to investigate behavioral changes over the course of infection. The *O. biroi - S. praecaptivus* system enables a fluorescence-based, non-lethal method for infection detection. With modifications to the current behavioral recording systems for *O. biroi* (Ulrich et al. 2018), this system can be used to investigate how social interaction network parameters change as the infection progresses.

# References

Anbutsu H, Moriyama M, Nikoh N, Hosokawa T, Futahashi R, Tanahashi M, Meng X-Y, Kuriwada T, Mori N, Oshima K, et al. 2017. Small genome symbiont underlies cuticle hardness in beetles. Proc Natl Acad Sci. 114(40):E8382–E8391. doi:10.1073/pnas.1712857114.

Arakane Y, Noh MY, Asano T, Kramer KJ. 2016. Tyrosine Metabolism for Insect Cuticle Pigmentation and Sclerotization. In: Cohen E, Moussian B, editors. Extracellular Composite Matrices in Arthropods. Cham: Springer International Publishing. p. 165–220. [accessed 2025 Mar 25]. https://doi.org/10.1007/978-3-319-40740-1_6.

Azzami K, Ritter W, Tautz J, Beier H. 2012. Infection of honey bees with acute bee paralysis virus does not trigger humoral or cellular immune responses. Arch Virol. 157(4):689. doi:10.1007/s00705-012-1223-0.

de Bekker C, Das B. 2022. Hijacking time: How Ophiocordyceps fungi could be using ant host clocks to manipulate behavior. Parasite Immunol. 44(3):e12909. doi:10.1111/pim.12909.

Bizzell F, Pull CD. 2024. Ant queens cannibalise infected brood to contain disease spread and recycle nutrients. Curr Biol. 34(18):R848–R849. doi:10.1016/j.cub.2024.07.062.

Chari A, Oakeson KF, Enomoto S, Jackson DG, Fisher MA, Dale C. 2015. Phenotypic characterization of Sodalis praecaptivus sp. nov., a close non-insect-associated member of the Sodalis-allied lineage of insect endosymbionts. Int J Syst Evol Microbiol. 65(Pt_5):1400–1405. doi:10.1099/ijs.0.000091.

Chaston J, Goodrich-Blair H. 2010. Common trends in mutualism revealed by model associations between invertebrates and bacteria. FEMS Microbiol Rev. 34(1):41–58. doi:10.1111/j.1574-6976.2009.00193.x.

Clayton AL, Oakeson KF, Gutin M, Pontes A, Dunn DM, Niederhausern AC von, Weiss RB, Fisher M, Dale C. 2012. A Novel Human-Infection-Derived Bacterium Provides Insights into the Evolutionary Origins of Mutualistic Insect–Bacterial Symbioses. PLOS Genet. 8(11):e1002990. doi:10.1371/journal.pgen.1002990.

Cole EL, Bayne H, Rosengaus RB. 2020. Young but not defenceless: antifungal activity during embryonic development of a social insect. R Soc Open Sci. 7(8):191418. doi:10.1098/rsos.191418.

Collins TJ. 2007. ImageJ for Microscopy. BioTechniques. 43(sup1):S25–S30. doi:10.2144/000112517.

Craggs JK, Ball JK, Thomson BJ, Irving WL, Grabowska AM. 2001. Development of a strand-specific RT-PCR based assay to detect the replicative form of hepatitis C virus RNA. J Virol Methods. 94(1):111–120. doi:10.1016/S0166-0934(01)00281-6.

Cremer S. 2019. Social immunity in insects. Curr Biol. 29(11):R458–R463. doi:10.1016/j.cub.2019.03.035.

Cremer S, Armitage SAO, Schmid-Hempel P. 2007. Social Immunity. Curr Biol.

17(16):R693–R702. doi:10.1016/j.cub.2007.06.008.

De Miranda JR, Cordoni G, Budge G. 2010. The Acute bee paralysis virus–Kashmir bee virus–Israeli acute paralysis virus complex. J Invertebr Pathol. 103:S30–S47. doi:10.1016/j.jip.2009.06.014.

Diez L, Urbain L, Lejeune P, Detrain C. 2015. Emergency measures: Adaptive response to pathogen intrusion in the ant nest. Behav Processes. 116:80–86. doi:10.1016/j.beproc.2015.04.016.

Flenniken ML, Andino R. 2013. Non-Specific dsRNA-Mediated Antiviral Response in the Honey Bee. PLOS ONE. 8(10):e77263. doi:10.1371/journal.pone.0077263.

Gammon DB, Mello CC. 2015. RNA interference-mediated antiviral defense in insects. Curr Opin Insect Sci. 8:111–120. doi:10.1016/j.cois.2015.01.006.

Gibson AK. 2022. Genetic diversity and disease: the past, present and future of an old idea. Evol Int J Org Evol. 76(Suppl 1):20–36. doi:10.1111/evo.14395.

Grangeasse C, Nessler S, Mijakovic I. 2012. Bacterial tyrosine kinases: evolution, biological function and structural insights. Philos Trans R Soc B Biol Sci. 367(1602):2640–2655. doi:10.1098/rstb.2011.0424.

Heinze J, Walter B. 2010. Moribund ants leave their nests to die in social isolation. Curr Biol CB. 20(3):249–252. doi:10.1016/j.cub.2009.12.031.

Hosokawa T, Koga R, Kikuchi Y, Meng X-Y, Fukatsu T. 2010. Wolbachia as a bacteriocyte-associated nutritional mutualist. Proc Natl Acad Sci U S A. 107(2):769–774. doi:10.1073/pnas.0911476107.

Jackson R, Monnin D, Patapiou PA, Golding G, Helanterä H, Oettler J, Heinze J, Wurm Y, Economou CK, Chapuisat M, et al. 2022. Convergent evolution of a labile nutritional symbiosis in ants. ISME J. 16(9):2114–2122. doi:10.1038/s41396-022-01256-1.

James W. Baty, Mariana Bulgarella, Jana Dobelmann, Antoine Felden & Philip J. Lester. 2020 Oct 21. Viruses and their effects in ants (Hymenoptera: Formicidae). Myrmecol News. doi:10.25849/myrmecol.news_030:213.

Jud SL, Knebel D, Ulrich Y. 2022. Intergenerational genotypic interactions drive collective behavioural cycles in a social insect. Proc Biol Sci. 289(1986):20221273. doi:10.1098/rspb.2022.1273.

Kaur N, Dey P. 2023. Bacterial exopolysaccharides as emerging bioactive macromolecules: from fundamentals to applications. Res Microbiol. 174(4):104024. doi:10.1016/j.resmic.2022.104024.

Konrad M, Vyleta ML, Theis FJ, Stock M, Tragust S, Klatt M, Drescher V, Marr C, Ugelvig LV, Cremer S. 2012. Social Transfer of Pathogenic Fungus Promotes Active Immunisation in Ant Colonies. PLOS Biol. 10(4):e1001300. doi:10.1371/journal.pbio.1001300.

Kronauer DJC, Pierce NE, Keller L. 2012. Asexual reproduction in introduced and native

populations of the ant erapachys biroi. Mol Ecol. 21(21):5221–5235. doi:10.1111/mec.12041.

LeBoeuf AC. 2017. Trophallaxis. Curr Biol. 27(24):R1299–R1300. doi:10.1016/j.cub.2017.10.047.

LeBoeuf AC, Waridel P, Brent CS, Gonçalves AN, Menin L, Ortiz D, Riba-Grognuz O, Koto A, Soares ZG, Privman E, et al. 2016. Oral transfer of chemical cues, growth proteins and hormones in social insects. Dicke M, editor. eLife. 5:e20375. doi:10.7554/eLife.20375.

Lester PJ, Buick KH, Baty JW, Felden A, Haywood J. 2019. Different bacterial and viral pathogens trigger distinct immune responses in a globally invasive ant. Sci Rep. 9(1):5780. doi:10.1038/s41598-019-41843-5.

Li Z, Bhat B, Frank ET, Oliveira-Honorato T, Azuma F, Bachmann V, Parker DJ, Schmitt T, Economo EP, Ulrich Y. 2023. Behavioural individuality determines infection risk in clonal ant colonies. Nat Commun. 14(1):5233. doi:10.1038/s41467-023-40983-7.

Little AEF, Murakami T, Mueller UG, Currie CR. 2003. The infrabuccal pellet piles of fungus-growing ants. Naturwissenschaften. 90(12):558–562. doi:10.1007/s00114-003-0480-x.

Livak KJ, Schmittgen TD. 2001. Analysis of Relative Gene Expression Data Using Real-Time Quantitative PCR and the 2−ΔΔCT Method. Methods. 25(4):402–408. doi:10.1006/meth.2001.1262.

Louten J. 2016. Virus Transmission and Epidemiology. Essent Hum Virol.:71–92. doi:10.1016/B978-0-12-800947-5.00005-3.

Mahanta DK, Bhoi TK, Komal J, Samal I, Nikhil RM, Paschapur AU, Singh G, Kumar PVD, Desai HR, Ahmad MA, et al. 2023. Insect-pathogen crosstalk and the cellular-molecular mechanisms of insect immunity: uncovering the underlying signaling pathways and immune regulatory function of non-coding RNAs. Front Immunol. 14:1169152. doi:10.3389/fimmu.2023.1169152.

Meunier J. 2015. Social immunity and the evolution of group living in insects. Philos Trans R Soc B Biol Sci. 370(1669):20140102. doi:10.1098/rstb.2014.0102.

Oxley PR, Ji L, Fetter-Pruneda I, McKenzie SK, Li C, Hu H, Zhang G, Kronauer DJC. 2014. The Genome of the Clonal Raider Ant Cerapachys biroi. Curr Biol. 24(4):451–458. doi:10.1016/j.cub.2014.01.018.

Payne AN, Shepherd TF, Rangel J. 2020. The detection of honey bee (Apis mellifera)-associated viruses in ants. Sci Rep. 10(1):2923. doi:10.1038/s41598-020-59712-x.

Pull CD, Ugelvig LV, Wiesenhofer F, Grasse AV, Tragust S, Schmitt T, Brown MJ, Cremer S. 2018. Destructive disinfection of infected brood prevents systemic disease spread in ant colonies. eLife. 7:e32073. doi:10.7554/eLife.32073.

Ramdya P, Schaffter T, Floreano D, Benton R. 2012. Fluorescence behavioral imaging (FBI) tracks identity in heterogeneous groups of Drosophila. PloS One. 7(11):e48381. doi:10.1371/journal.pone.0048381.

Ravary F, Jahyny B, Jaisson P. 2006. Brood stimulation controls the phasic reproductive cycle of the parthenogenetic ant Cerapachys biroi. Insectes Sociaux. 53(1):20–26. doi:10.1007/s00040-005-0828-7.

Ravary F, Jaisson P. 2002. The reproductive cycle of thelytokous colonies of Cerapachys biroi Forel (Formicidae, Cerapachyinae). Insectes Sociaux. 49(2):114–119. doi:10.1007/s00040-002-8288-9.

Ravary F, Jaisson P. 2004. Absence of individual sterility in thelytokous colonies of the ant Cerapachys biroi Forel (Formicidae, Cerapachyinae). Insectes Sociaux. 51(1):67–73. doi:10.1007/s00040-003-0724-y.

Renoz F, Arai H, Pons I. 2024. The genus Sodalis as a resource for understanding the multifaceted evolution of bacterial symbiosis in insects. Symbiosis. 92(2):187–208. doi:10.1007/s13199-023-00966-0.

Rosenberg Y, Bar-On YM, Fromm A, Ostikar M, Shoshany A, Giz O, Milo R. 2023. The global biomass and number of terrestrial arthropods. Sci Adv. 9(5):eabq4049. doi:10.1126/sciadv.abq4049.

Rueppell O, Hayworth MK, Ross NP. 2010. Altruistic self-removal of health-compromised honey bee workers from their hive. J Evol Biol. 23(7):1538–1546. doi:10.1111/j.1420-9101.2010.02022.x.

Sarkar A, McInroy CJA, Harty S, Raulo A, Ibata NGO, Valles-Colomer M, Johnson KV-A, Brito IL, Henrich J, Archie EA, et al. 2024. Microbial transmission in the social microbiome and host health and disease. Cell. 187(1):17–43. doi:10.1016/j.cell.2023.12.014.

Schindelin J, Arganda-Carreras I, Frise E, Kaynig V, Longair M, Pietzsch T, Preibisch S, Rueden C, Saalfeld S, Schmid B, et al. 2012. Fiji: an open-source platform for biological-image analysis. Nat Methods. 9(7):676–682. doi:10.1038/nmeth.2019.

Schläppi D, Chejanovsky N, Yañez O, Neumann P. 2020. Foodborne Transmission and Clinical Symptoms of Honey Bee Viruses in Ants Lasius spp. Viruses. 12(3):321. doi:10.3390/v12030321.

Schmid-Hempel P. 1995. Parasites and social insects. Apidologie. 26(3):255–271. doi:10.1051/apido:19950307.

Schmid-Hempel P. 1998. Parasites in Social Insects. Princeton University Press.

Schultheiss P, Nooten SS, Wang R, Wong MKL, Brassard F, Guénard B. 2022. The abundance, biomass, and distribution of ants on Earth. Proc Natl Acad Sci. 119(40):e2201550119. doi:10.1073/pnas.2201550119.

Schuster S, Miesen P, van Rij RP. 2019. Antiviral RNAi in Insects and Mammals: Parallels and Differences. Viruses. 11(5):448. doi:10.3390/v11050448.

Searle CL, Xie GY, Blaustein AR. 2013. Development and Infectious Disease in Hosts with Complex Life Cycles. PLOS ONE. 8(4):e60920. doi:10.1371/journal.pone.0060920.

Shykoff JA, Schmid-Hempel P. 1997. Parasites and the advantage of genetic variability within social insect colonies. Proc R Soc Lond B Biol Sci. 243(1306):55–58. doi:10.1098/rspb.1991.0009.

Smith DFQ, Dragotakes Q, Kulkarni M, Hardwick JM, Casadevall A. 2022. Galleria mellonella immune melanization is fungicidal during infection. Commun Biol. 5:1364. doi:10.1038/s42003-022-04340-6.

Snir O, Alwaseem H, Heissel S, Sharma A, Valdés-Rodríguez S, Carroll TS, Jiang CS, Razzauti J, Kronauer DJC. 2022. The pupal moulting fluid has evolved social functions in ants. Nature. 612(7940):488–494. doi:10.1038/s41586-022-05480-9.

Starks PT, Blackie CA, Seeley TD. 2000. Fever in honeybee colonies. Naturwissenschaften. 87(5):229–231. doi:10.1007/s001140050709.

Stroeymeyt N, Grasse AV, Crespi A, Mersch DP, Cremer S, Keller L. 2018. Social network plasticity decreases disease transmission in a eusocial insect. Science. 362(6417):941–945. doi:10.1126/science.aat4793.

Su Y, Lin H-C, Dale C. 2023. Protocol to establish a genetically tractable synthetic symbiosis between *Sodalis praecaptivus* and grain weevils by insect egg microinjection. STAR Protoc. 4(2):102156. doi:10.1016/j.xpro.2023.102156.

Su Y, Lin H-C, Teh LS, Chevance F, James I, Mayfield C, Golic KG, Gagnon JA, Rog O, Dale C. 2022. Rational engineering of a synthetic insect-bacterial mutualism. Curr Biol. 32(18):3925-3938.e6. doi:10.1016/j.cub.2022.07.036.

Sun Q, Zhou X. 2013. Corpse Management in Social Insects. Int J Biol Sci. 9(3):313–321. doi:10.7150/ijbs.5781.

Tantillo G, Bottaro M, Di Pinto A, Martella V, Di Pinto P, Terio V. 2015. Virus Infections of Honeybees Apis Mellifera. Ital J Food Saf. 4(3):5364. doi:10.4081/ijfs.2015.5364.

Tehel A, Streicher T, Tragust S, Paxton RJ. 2022. Experimental cross species transmission of a major viral pathogen in bees is predominantly from honeybees to bumblebees. Proc R Soc B Biol Sci. 289(1969):20212255. doi:10.1098/rspb.2021.2255.

Tehel A, Vu Q, Bigot D, Gogol-Döring A, Koch P, Jenkins C, Doublet V, Theodorou P, Paxton R. 2019. The Two Prevalent Genotypes of an Emerging Infectious Disease, Deformed Wing Virus, Cause Equally Low Pupal Mortality and Equally High Wing Deformities in Host Honey Bees. Viruses. 11(2):114. doi:10.3390/v11020114.

Theis FJ, Ugelvig LV, Marr C, Cremer S. 2015. Opposing effects of allogrooming on disease transmission in ant societies. Philos Trans R Soc B Biol Sci. 370(1669):20140108. doi:10.1098/rstb.2014.0108.

Trible W, Olivos-Cisneros L, McKenzie SK, Saragosti J, Chang N-C, Matthews BJ, Oxley PR, Kronauer DJC. 2017. orco Mutagenesis Causes Loss of Antennal Lobe Glomeruli and Impaired Social Behavior in Ants. Cell. 170(4):727-735.e10. doi:10.1016/j.cell.2017.07.001.

Ulrich Y, Saragosti J, Tokita CK, Tarnita CE, Kronauer DJC. 2018. Fitness benefits and

emergent division of labour at the onset of group living. Nature. 560(7720):635–638. doi:10.1038/s41586-018-0422-6.

Vaibhvi V, Künzel S, Roeder T. 2022. Hemocytes and fat body cells, the only professional immune cell types in Drosophila, show strikingly different responses to systemic infections. Front Immunol. 13. doi:10.3389/fimmu.2022.1040510. [accessed 2025 Mar 12]. https://www.frontiersin.org/journals/immunology/articles/10.3389/fimmu.2022.1040510/full.

vanEngelsdorp D, Evans JD, Saegerman C, Mullin C, Haubruge E, Nguyen BK, Frazier M, Frazier J, Cox-Foster D, Chen Y, et al. 2009. Colony Collapse Disorder: A Descriptive Study. PLOS ONE. 4(8):e6481. doi:10.1371/journal.pone.0006481.

Viljakainen L, Fürst MA, Grasse AV, Jurvansuu J, Oh J, Tolonen L, Eder T, Rattei T, Cremer S. 2023. Antiviral immune response reveals host-specific virus infections in natural ant populations. Front Microbiol. 14. doi:10.3389/fmicb.2023.1119002. [accessed 2024 Oct 20]. https://www.frontiersin.org/journals/microbiology/articles/10.3389/fmicb.2023.1119002/full.

Weiss B, Kaltenpoth M. 2016. Bacteriome-Localized Intracellular Symbionts in Pollen-Feeding Beetles of the Genus Dasytes (Coleoptera, Dasytidae). Front Microbiol. 7. doi:10.3389/fmicb.2016.01486. [accessed 2025 Mar 16]. https://www.frontiersin.org/journals/microbiology/articles/10.3389/fmicb.2016.01486/full.

Weiss B, Shalom SR, Dolgova A, Teh LS, Kaltenpoth M, Dale C, Chiel E. 2025. Maternal symbiont transmission via envenomation in the parasitoid wasp Spalangia cameroni. Curr Biol. 0(0). doi:10.1016/j.cub.2025.02.035. [accessed 2025 Mar 16]. https://www.cell.com/current-biology/abstract/S0960-9822(25)00199-X.

Westhus C, Ugelvig LV, Tourdot E, Heinze J, Doums C, Cremer S. 2014. Increased grooming after repeated brood care provides sanitary benefits in a clonal ant. Behav Ecol Sociobiol. 68(10):1701–1710. doi:10.1007/s00265-014-1778-8.

Whitten MMA, Coates CJ. 2017. Re-evaluation of insect melanogenesis research: Views from the dark side. Pigment Cell Melanoma Res. 30(4):386–401. doi:10.1111/pcmr.12590.

Wierz JC, Gimmel ML, Huthmacher S, Engl T, Kaltenpoth M. 2024. Evolutionary history of tyrosine-supplementing endosymbionts in pollen-feeding beetles. ISME J. 18(1):wrae080. doi:10.1093/ismejo/wrae080.

Wilson, E.O. 1971. The Insect Societies. Harvard University Press, Cambridge, Massachussetts, 1971.

Wilson-Rich N, Spivak M, Fefferman NH, Starks PT. 2009. Genetic, Individual, and Group Facilitation of Disease Resistance in Insect Societies. Annu Rev Entomol. 54(Volume 54, 2009):405–423. doi:10.1146/annurev.ento.53.103106.093301.

Yamaguchi S, Naganuma M, Nishizawa T, Kusakizako T, Tomari Y, Nishimasu H, Nureki O. 2022. Structure of the Dicer-2-R2D2 heterodimer bound to a small RNA duplex. Nature. 607(7918):393–398. doi:10.1038/s41586-022-04790-2.

Zdybicka-Barabas A, Stączek S, Kunat-Budzyńska M, Cytryńska M. 2025. Innate Immunity in Insects: The Lights and Shadows of Phenoloxidase System Activation. Int J Mol Sci.

26(3):1320. doi:10.3390/ijms26031320.

# Supplementary

## Figures

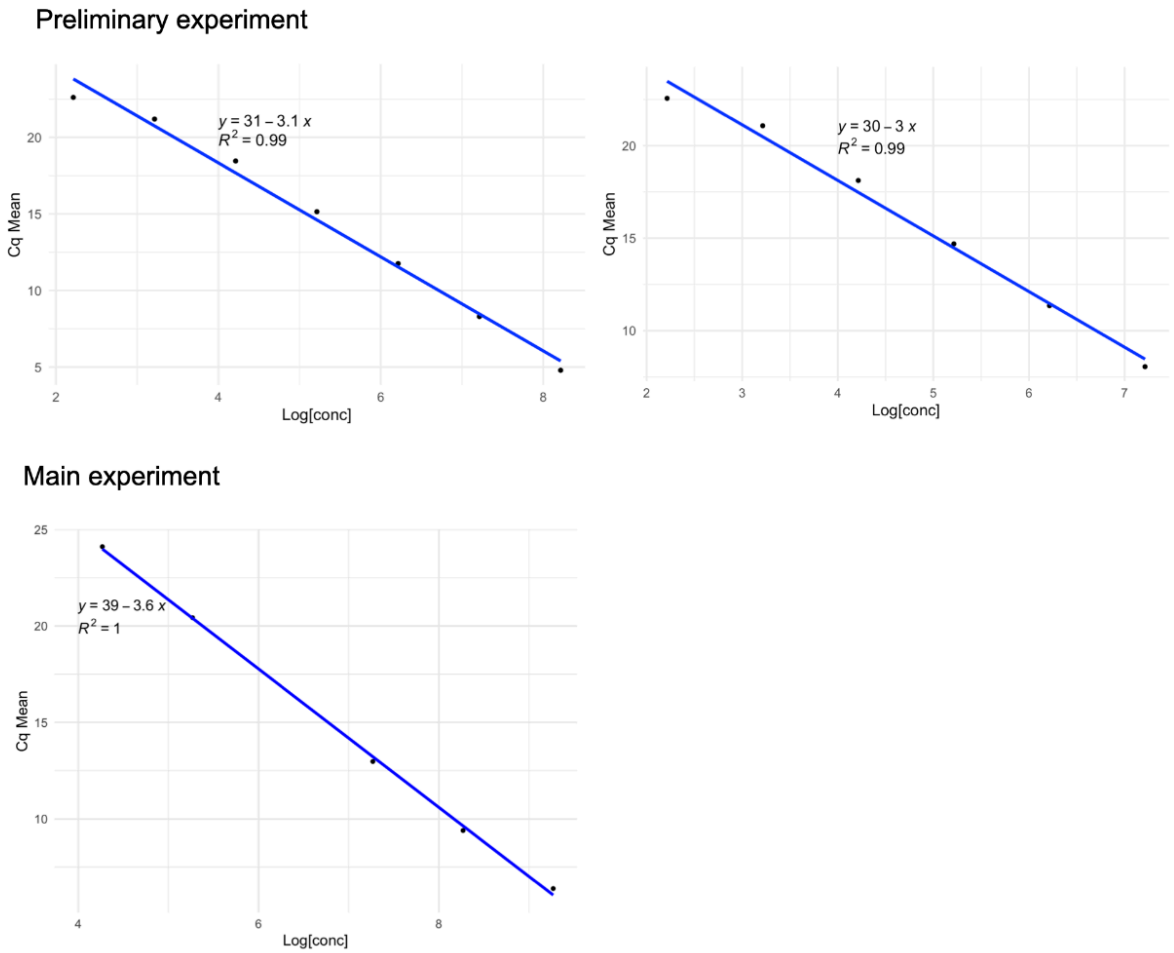


S1. Standard curves used for qPCR analysis of the viral load: The preliminary experiment had two separate qPCR plates hence, two separate standard curves were made. x-axis represents the log of concentration of viral DNA

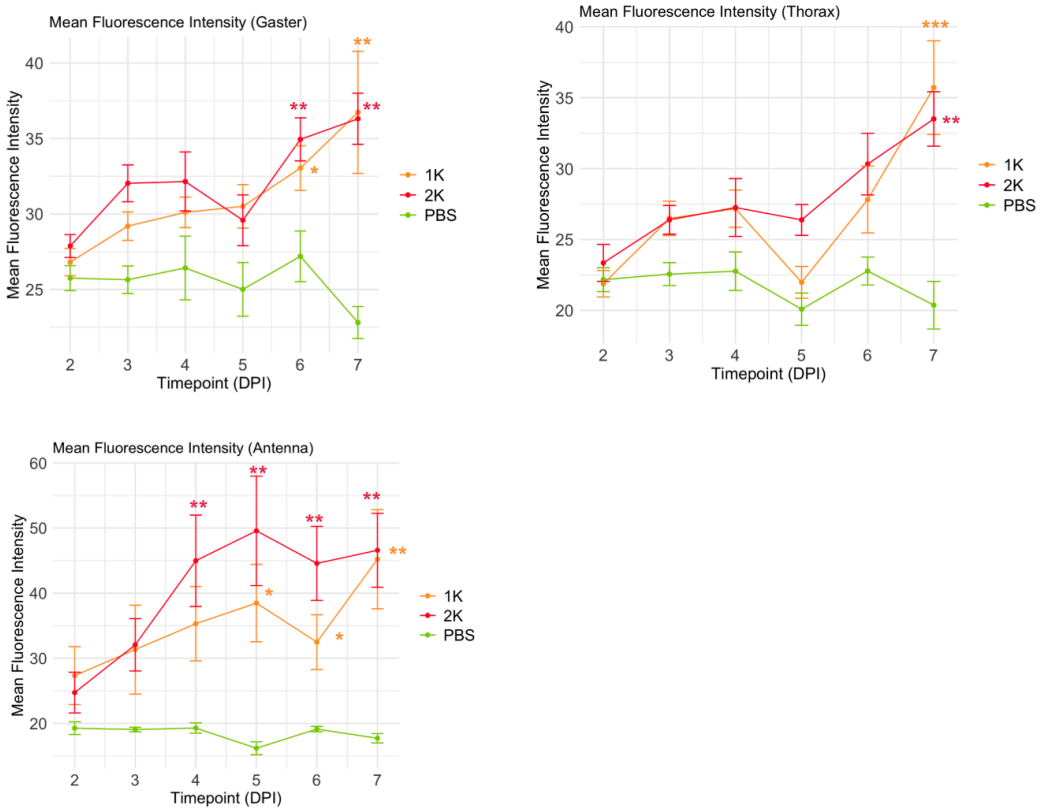


S2: Area-wise change in fluorescent intensity of adult *O. biroi* adults after *S. praecaptivus* injection from 1K represents adults injected with 1000 *S. praecaptivus* cells, 2K represents adults injected with 2000 *S. praecaptivus* cells, PBS represents adults injected with PBS, DPI - 2 to DPI - 7 '***' $p < 0.001$ '**' $p < 0.01$ '*' $p < 0.05$ 'NS' nonsignificant, asterisk colour symbolizes the group that is significant compared to PBS.

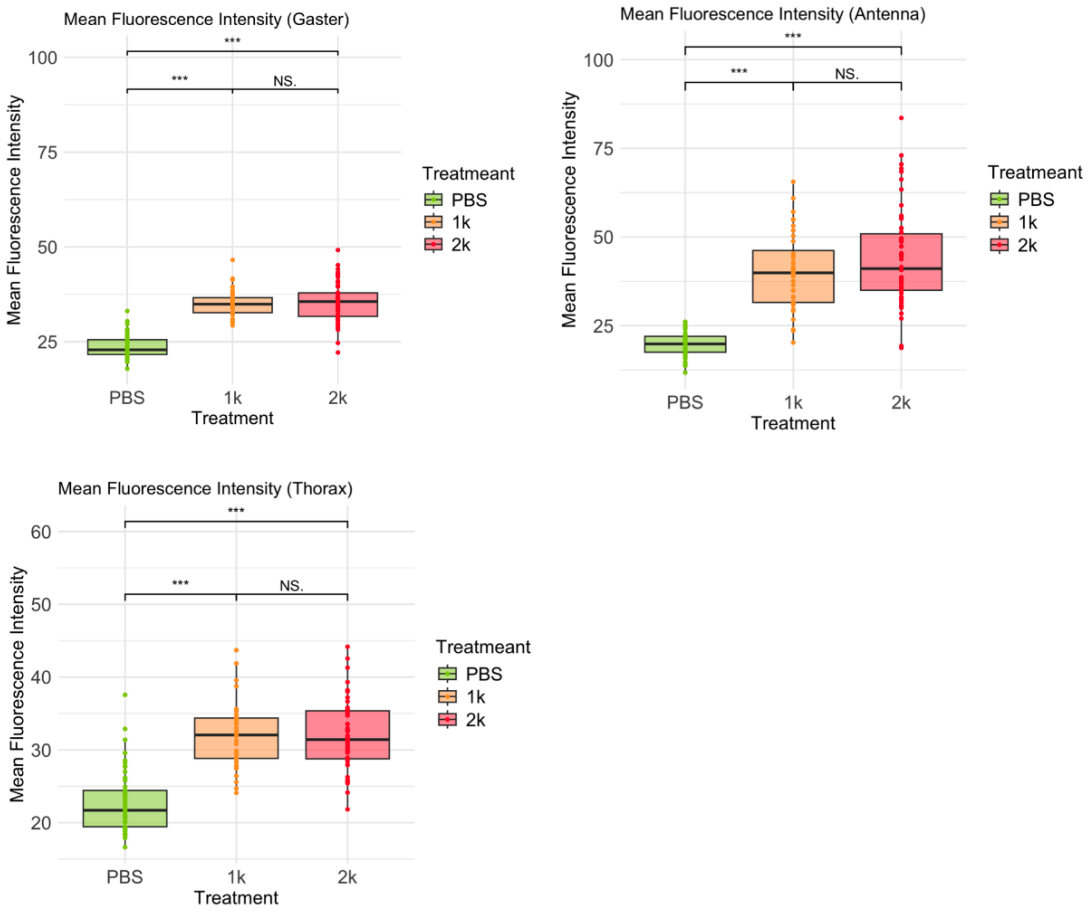


S3: Area-wise change in fluorescent intensity of adult *O. biroi* adults after eight days after *S. praecaptivus* injection, 1K represents adults injected with 1000 *S. praecaptivus* cells, 2K represents adults injected with 2000 *S. praecaptivus* cells, PBS represents adults injected with PBS; '***' $p < 0.001$ '**' $p < 0.01$ '*' $p < 0.05$ 'NS' nonsignificant (2K.I: n = 54, 1K.I: n = 40, PBS.I: n = 56)

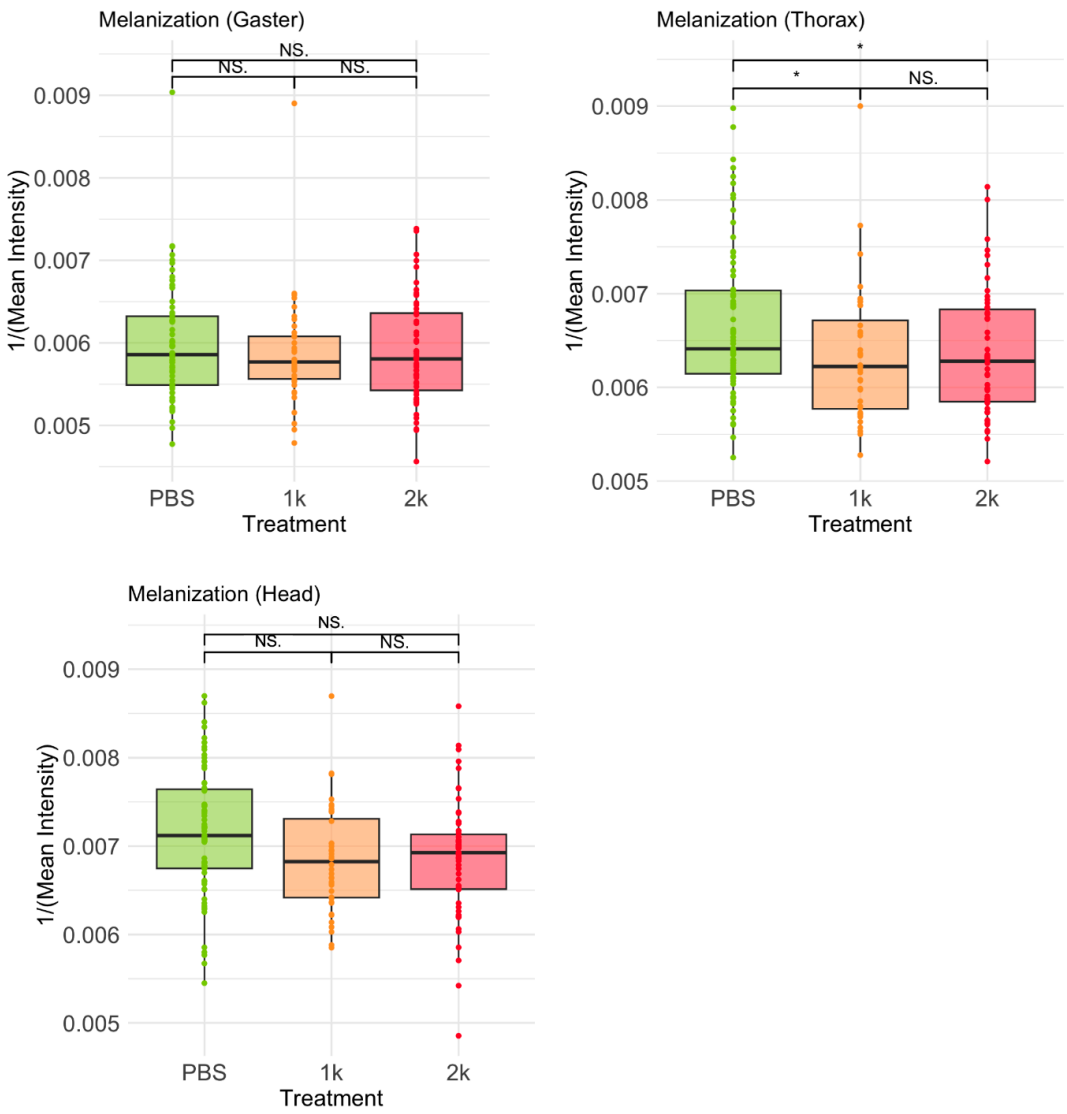


S4: Area-wise change is melanization of *S. praecaptivus* injected ants at DPI - 8; (2K.I: n = 54, 1K.I: n = 40, PBS.I: n = 72), 1K represents adults injected with 1000 *S. praecaptivus* cells, 2K represents adults injected with 2000 *S. praecaptivus* cells, PBS represents adults injected with PBS '***' $p < 0.001$ '**' $p < 0.01$ '*' $p < 0.05$ 'NS' nonsignificant

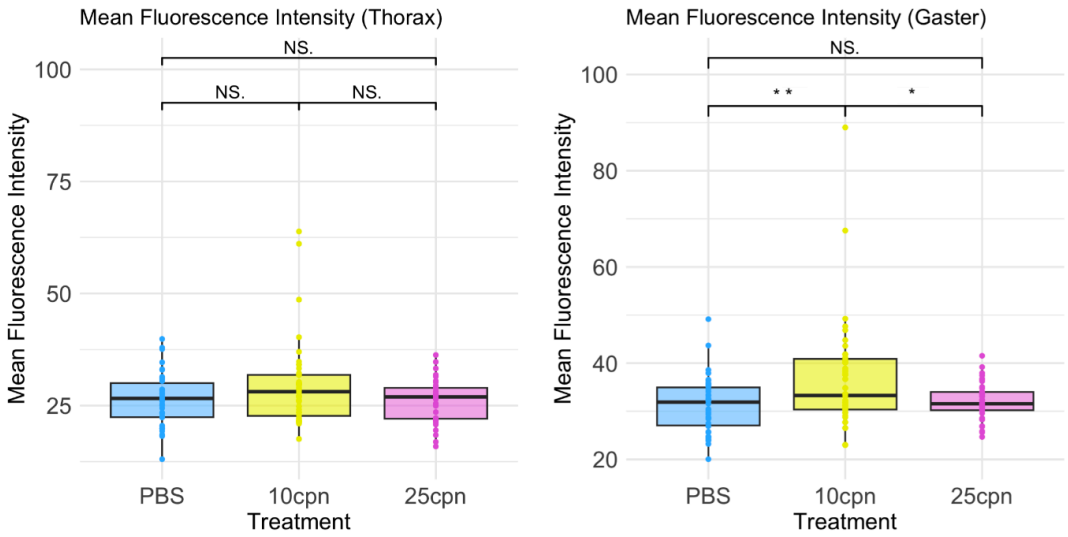


S5: Areawise change is the fluorescence of adults cohabitating *S. praecaptivus* injected pupae at DPI - 8; (25cpn.CH: n = 38, represents adults cohabitating pupae injected with 25 cell/nL, 10cpn.CH: n = 44, represents adults cohabitating pupae injected with 10 cell/nL, PBS.CH: n = 42, represents adults cohabitating pupae injected with PBS); '***' $p < 0.001$ '**' $p < 0.01$ '*' $p < 0.05$ 'NS' nonsignificant

# R - Code

The codes used for analysis of the data are recorded here. Small changes in these codes were made to incorporate differences in various datasets.

## Code for measuring viral load:

```
library(dplyr)
library(pcr)
library(ggplot2)
library(tidyr)
library(multcomp)
library(ggpubr)
library(scales)
#setting the working directory
setwd("/Users/ashmitabaruah/Desktop/MPI_CE/Stats/fABPV")
```

```
#Making the Standard Curve
#naming the file I am going to work with
fvl<- read.csv('Infection4 - StandardCurve_Inf4.csv')
View(fvl)
filter(!grepl(c("Std7","Std8"), Sample))
summary(fvl)
View(fvl)
fvl_std<- ggplot(fvl, aes(x = Log, y = EqCq_Mean)) +
  geom_point(size = 1) +  # Plot points
  geom_smooth(method = "lm", se = FALSE, color = "blue") +  # Fit a linear model
(standard curve)
  labs(x = "Log[conc]", y = "Cq Mean", title = "Standard Curve 1") +
  theme_minimal()+
  stat_regline_equation(label.x = 4, label.y = 21) +  # Add regression equation
  stat_cor(label.x = 4, label.y = 20, aes(label = paste(after_stat(rr.label), sep = "")))
print(fvl_std)

color_mapping <- c(
  "ABPV.I" = "brown1",
  "ABPV.CH" = "orchid",
  "Bee-extract.I" = "yellowgreen",
  "Bee-extract.CH" = "steelblue1",
  "Uninjected." = "grey"
)

fvl2<- read.csv('Infection4 - Clean.csv')
fvl2 <- fvl2 %>%
  mutate(Group = interaction(Treatment, Type, sep = "."))
fvl2$Group <- factor(fvl2$Group, levels = c("ABPV.I", "ABPV.CH", "Bee-extract.I",
"Bee-extract.CH", "Uninjected."))

plotfvlge_1 <- ggplot(fvl2, aes(x = as.factor(TimePoint), y = Dil_Rem_ge, fill = Group)) +
  geom_boxplot(alpha = 0.5, outlier.shape = NA) +  # Boxplot without outlier dots (to
avoid duplication)
  geom_point(aes(color = Group),
             position = position_dodge(width = 0.75),  # Align points with boxplots
             alpha = 1, size = 1) +  # Adjust transparency & size
  labs(x = "Timepoint (hrs post injection)", y = "Viral Load (ge/µL)", title = "ABPV Load in
All Adults") +
```

```
  scale_fill_manual(values = color_mapping) +
  scale_color_manual(values = color_mapping) +  # Ensure points match boxplot colors
  scale_y_continuous(limits = c(0, 1250)) +  # Set y-axis range from 0 to 4000
  theme_minimal() +
  theme(
    axis.title = element_text(family = "Arial", size = 14),  # Axis labels font
    axis.text = element_text(family = "Arial", size = 14),  # Axis tick labels font
    legend.title = element_text(family = "Arial", size = 14),  # Legend title font
    legend.text = element_text(family = "Arial", size = 14)  # Legend labels font
  )

plotfvlge_1


# Filter dataset for only the Focal groups
fvl2_I <- fvl2 %>%
  filter(Group %in% c("ABPV.I", "Bee-extract.I"))

# Create the box plot with filtered data
plotfvlge_I <- ggplot(fvl2_I, aes(x = as.factor(TimePoint), y = Dil_Rem_ge, fill = Group))
+
  geom_boxplot(alpha = 0.5, outlier.shape = NA) +  # Boxplot without outlier dots
  geom_point(aes(color = Group),
             position = position_dodge(width = 0.75),  # Align points with boxplots
             alpha = 1, size = 1) +  # Adjust transparency & size
  labs(x = "Timepoint (hrs post injection)", y = "Viral Load (ge/µL)", title = "ABPV Load in
ABPV.I & Bee-extract.I") +
  scale_fill_manual(values = color_mapping) +
  scale_color_manual(values = color_mapping) +  # Ensure points match boxplot colors
  theme_minimal() +
  theme(
    axis.title = element_text(family = "Arial", size = 14),  # Axis labels font
    axis.text = element_text(family = "Arial", size = 14),  # Axis tick labels font
    legend.title = element_text(family = "Arial", size = 14),  # Legend title font
    legend.text = element_text(family = "Arial", size = 14)  # Legend labels font
  )
plotfvlge_I

# Filter dataset for only the desired groups
fvl2_CH <- fvl2 %>%
```

```
  filter(Group %in% c("ABPV.CH", "Bee-extract.CH"))

# Filter dataset for only the desired groups
fvl2_CH <- fvl2 %>%
  filter(Group %in% c("ABPV.CH", "Bee-extract.CH"))

# Create the box plot with only CH
plotfvlge_CH <- ggplot(fvl2_CH, aes(x = as.factor(TimePoint), y = Dil_Rem_ge, fill =
Group)) +
  geom_boxplot(alpha = 0.5, outlier.shape = NA) +  # Boxplot without outlier dots
  geom_point(aes(color = Group),
             position = position_dodge(width = 0.75),  # Align points with boxplots
             alpha = 1, size = 1) +  # Adjust transparency & size
  labs(x = "Timepoint (hrs post exposure)", y = "Viral Load (ge/µL)", title = "ABPV Load
in ABPV.CH & Bee-extract.CH") +
  scale_fill_manual(values = color_mapping) +
  scale_color_manual(values = color_mapping) +  # Ensure points match boxplot colors
  scale_y_continuous(limits = c(0, 1250), breaks = seq(0, 1250, by = 250)) +  # Set
y-axis range
  theme_minimal() +
  theme(
    axis.title = element_text(family = "Arial", size = 14),  # Axis labels font
    axis.text = element_text(family = "Arial", size = 14),  # Axis tick labels font
    legend.title = element_text(family = "Arial", size = 14),  # Legend title font
    legend.text = element_text(family = "Arial", size = 14)  # Legend labels font
  )
# Display the plot
plotfvlge_CH

fvl2_I <- fvl2 %>%
  filter(!grepl("CH", Type))
fvl2_I

# Two-way ANOVA
anova_result_vl_F <- aov(Dil_Rem_ge ~ Treatment*TimePoint, data = fvl2_I)
residuals_anova <- residuals(anova_result_vl_F)
shapiro_test <- shapiro.test(residuals_anova)
print(shapiro_test)

scheirer_test <- scheirerRayHare(Dil_Rem_ge ~ Treatment * TimePoint, data = fvl2_I)
```

```
# Print results
print(scheirer_test)
pairwise_results <- fvl2_I %>%
  group_by(TimePoint) %>%
  pairwise_wilcox_test(Dil_Rem_ge ~ Treatment, p.adjust.method = "bonferroni")
# Print the results
print(pairwise_results)

fvl2_I
# Perform Kruskal-Wallis test separately for each timepoint
kruskal_results <- fvl2 %>%
  group_by(TimePoint) %>%
  summarise(
    test_result = list(kruskal.test(Dil_Rem_ge ~ Treatment, data = cur_data()))
  )
print(kruskal_results)
# Print the Kruskal-Wallis test results for each Timepoint
kruskal_results %>% pull(test_result)

summary(anova_result_vl_F)

# Tukey HSD post-hoc test for interaction
tukey_interaction_vl_F <- TukeyHSD(anova_result_vl_F, "TimePoint:Treatment")

# Print results
print(tukey_interaction_vl_F)

# Plot results for visualization
plot(tukey_interaction_vl_F)

fvl2_CH <- fvl2 %>%
  filter(!grepl("I", Type))
fvl2_CH
fvl2_U <- fvl2 %>%
  filter(Treatment == "Uninjected")
fvl2_U
fvl2_allCH <- rbind(fvl2_U, fvl2_CH)
fvl2_allCH
fvl2_allCH %>%
```

```
  filter(TimePoint != 0) %>%  # Remove TimePoint = 0
  group_by(TimePoint) %>%
  pairwise_wilcox_test(Dil_Rem_ge ~ Treatment, p.adjust.method = "bonferroni") %>%
  print()
# Two-way ANOVA
anova_result_vl_CH <- aov(Dil_Rem_ge ~ TimePoint * Treatment, data = fvl2_allCH)

# Summary of the ANOVA results
summary(anova_result_vl_CH)

residuals_anova <- residuals(anova_result_vl_CH)
shapiro_test <- shapiro.test(residuals_anova)
print(shapiro_test)

scheirer_test <- scheirerRayHare(Dil_Rem_ge ~ Treatment * TimePoint, data =
fvl2_allCH)

table(fvl2_allCH$TimePoint, fvl2_allCH$Treatment)
# Print results
print(scheirer_test)
pairwise_results <- fvl2_allCH %>%
  group_by(TimePoint) %>%
  pairwise_wilcox_test(Dil_Rem_ge ~ Treatment, p.adjust.method = "bonferroni")
# Print the results
print(pairwise_results)

# Tukey HSD post-hoc test for interaction
tukey_interaction_vl_CH <- TukeyHSD(anova_result_vl_CH, "TimePoint:Treatment")
# Print results
print(tukey_interaction_vl_CH)
# Plot results for visualization
plot(tukey_interaction_vl_CH)
```

## Code for *Dcr-2* expression levels

```
library(dplyr)
library(pcr)
library(ggplot2)
library(tidyr)
library(multcomp)
```

```
#setting the working directory
setwd("/Users/ashmitabaruah/Desktop/MPI_CE/Stats/fABPV")
#naming the file I am going to work with
fdcr2<- read.csv('20241025_Ash_fABPV_Dcr2 - RelCompiled.csv')
#converting the groups based on what I want to seggreate into factors
fdcr2$Treatment <- factor(fdcr2$Treatment)
fdcr2$Target <- factor(fdcr2$Target)
fdcr2$TimePoint <- factor(fdcr2$TimePoint)
fdcr2
#Remove all the RPF columns
fdcr2_filtered <- fdcr2 %>%
  filter(!grepl("RPF-13a", Target))
print(fdcr2_filtered)

#creating the new table for the with grouping
mean.data2<- c()
mean.data2<- fdcr2_filtered%>%
  group_by(Treatment, TimePoint, Type)%>%
  summarize(count = n(),
            mean_value = -mean(Delta.EqCq.Mean),
            sd_value = sd(Delta.EqCq.Mean),
            se_value = sd_value/sqrt(length(Delta.EqCq.Mean))
  )
mean.data2
#arranging necessary to make the line plot
mean.data2 <- mean.data2 %>%
  arrange(TimePoint,Type)
print(mean.data2)
#Part where you get the final figure
# Create baseline values for each TimePoint from the Uninjected group
baseline <- mean.data2 %>%
  filter(Treatment == "Uninjected") %>%
  group_by(TimePoint) %>%
  summarize(baseline_mean = mean(mean_value), baseline_sd = mean(sd_value))
baseline

# Join baseline values with ABPV and BE data, then calculate the difference
diff_table <- mean.data2 %>%
  filter(Treatment %in% c("ABPV", "Bee-extract")) %>%
```

```
  left_join(baseline, by = "TimePoint") %>%
  mutate(
    rel_exp2 = 2^(mean_value - baseline_mean),         # Difference from untreated mean
    sd_diff = sqrt(sd_value^2 + baseline_sd^2),
    se_diff = sd_diff/sqrt(count),                     # Combined standard error
    Treatment_Type = paste(Treatment, Type, sep = ".")  # Create a unique label for each
combination
  )
diff_table
diff_table$Treatment_Type <- factor(diff_table$Treatment_Type, levels =
c("ABPV.I","ABPV.CH","Bee-extract.I", "Bee-extract.CH"))

# Define custom colors for each Treatment-Type combination
color_mapping <- c(
  "ABPV.I" = "indianred1",
  "ABPV.CH" = "orchid",
  "Bee-extract.I" = "yellowgreen",
  "Bee-extract.CH" = "steelblue1"
)

plot4 <- ggplot(diff_table, aes(x = TimePoint, y = rel_exp2, fill = Treatment_Type)) +
  geom_bar(stat = "identity", position = position_dodge(width = 0.7), alpha = 0.8) +
  geom_errorbar(aes(ymin = rel_exp2 - se_diff, ymax = rel_exp2 + se_diff),
                alpha = 0.3, width = 0.5, position = position_dodge(width = 0.7)) +
  geom_hline(yintercept = 1, linetype = "solid", color = "black", size = 0.5) +  # Adjusted
baseline
  labs(y = "Fold change in Dcr-2 w.r.t control",
       x = "Timepoint (hrs post injection)",
       title = "Fold change in Dcr-2 w.r.t.uninjected control",
       fill = "Group") +
  theme_minimal() +
  theme(
    axis.title = element_text(family = "Arial", size = 14),  # Axis labels font
    axis.text = element_text(family = "Arial", size = 14),
    axis.text.x = element_text(size = 14),
    axis.text.y = element_text(size = 14),
    legend.title = element_text(family = "Arial", size = 14),
    legend.text = element_text(family = "Arial", size = 14)
  ) +
  scale_fill_manual(values = color_mapping) +  # Custom color
```

```
  scale_y_continuous(limits = c(0, 2))  # Adjusted y-axis limits
```

Plot4

```
# Two-way ANOVA with interaction
anova_result_F_times <- aov(Delta.EqCq.Mean ~ TimePoint * Treatment, data =
fdcr2_allF)
summary(anova_result_F_times)
residuals_anova <- residuals(anova_result_F_times)
shapiro_test <- shapiro.test(residuals_anova)
print(shapiro_test)


# Tukey HSD post-hoc test for interaction
tukey_interaction <- TukeyHSD(anova_result_F_times, "TimePoint:Treatment")

# Print results
print(tukey_interaction)

# Plot results for visualization
plot(tukey_interaction)

# Two-way ANOVA without interaction
anova_result_F_plus <- aov(Delta.EqCq.Mean ~ TimePoint + Treatment, data =
fdcr2_allF)
summary(anova_result_F_plus)

# Run Tukey Honest Significance Difference for TimePoint
tukey_time <- TukeyHSD(anova_result_F_plus , "TimePoint")
tukey_treat <- TukeyHSD(anova_result_F_plus , "Treatment")

# View results
print(tukey_time)
print(tukey_treat)

# Separate ANOVA for each treatment
for (treat in unique(fdcr2_allF$Treatment)) {
  cat("\nANOVA results for Treatment", treat, "\n")

  # Subset data for the specific time point
```

```
  subset_treat_F <- subset(fdcr2_allF, Treatment == treat)

  # Two-way ANOVA with Timepoint as the factor
  anova_result_treat_F <- aov(Delta.EqCq.Mean ~ TimePoint, data = subset_treat_F)

  # Print the summary of the results
  print(summary(anova_result_treat_F))
}
```

## Code for Fluorescence analysis of the time progression

```
library(ggplot2)
library(dplyr)
library(ggpubr)
library(ggsignif)
library(rcompanion)
library(rstatix)

setwd("/Users/ashmitabaruah/Desktop/MPI_CE/Stats/Sodalis/AdultDosageDependence
")
P13FI<- read.csv('Sodalis_PupaeInjections - DPI16_CH_Clean.csv')
# Ensure categorical variables are factors
P13FI$Treatmeant <- factor(P13FI$Treatmeant)
P13FI

P13FI_mean <- P13FI %>%
  group_by(Treatmeant) %>%
  summarise(
    mean_intensity = mean(Mean, na.rm = TRUE),
    se_intensity = sd(Mean, na.rm = TRUE) / sqrt(n()),
    mean_gaster = mean(Gaster_MeanI),
    se_gaster = sd(Gaster_MeanI, na.rm = TRUE) / sqrt(n()),
    mean_head = mean(Head_MeanI, na.rm = TRUE),
    se_head = sd(Head_MeanI, na.rm = TRUE) / sqrt(n()),
    mean_thorax = mean(Thorax_MeanI),
    se_thorax = sd(Thorax_MeanI, na.rm = TRUE) / sqrt(n()),
    mean_antenna = mean(Antenna_MeanI),
    se_antenna = sd(Antenna_MeanI, na.rm = TRUE) / sqrt(n()),
    n_replicates = n()
  )
```

```
P13FI_mean

custom_colors <- c(
  "25cpn" = "brown1",
  "10cpn" = "tan1",
  "PBS" = "yellowgreen"
  )

# Create the line graph with custom colors and fonts
ggplot(P13FI_mean, aes(x = DPI, y = mean_intensity, color = Treatmeant, group =
Treatmeant)) +
  geom_line() +  # Lines for each treatment
  geom_point() + # Add points at each DPI
  geom_errorbar(aes(ymin = mean_intensity - se_intensity, ymax = mean_intensity +
se_intensity), width = 0.2) +  # Error bars
  scale_y_continuous(limits = c(0, 200)) +
  scale_color_manual(values = custom_colors) +  # Apply custom colors
  labs(
    title = "Mean Fluorescence Intensity",
    x = "Timepoint (DPI)",
    y = "Mean Fluorescence Intensity"
  ) +
  theme_minimal() +  # Clean theme
  theme(
    axis.title = element_text(family = "Arial", size = 14),  # Axis labels font
    axis.text = element_text(family = "Arial", size = 14),  # Axis tick labels font
    legend.title = element_text(family = "Arial", size = 12),  # Legend title font
    legend.text = element_text(family = "Arial", size = 14)  # Legend labels font
  ) +
  theme(legend.title = element_blank())  # Remove legend title
class(P13FI)

anova_result_P13FI <- aov(Mean ~ Treatmeant, data = P13FI)
# Summary of the ANOVA results
summary(anova_result_P13FI)
residuals_anova <- residuals(anova_result_P13FI)
shapiro_test <- shapiro.test(residuals_anova)
print(shapiro_test)
```

```
summary(P13FI)
P13FI
scheirer_test <- scheirerRayHare(MeanI ~ Treatmeant, data = P13FI)

# Print results
print(scheirer_test)

post_hoc_test <- P13FI %>%
  group_by(DPI) %>%
  pairwise_wilcox_test(MeanI ~ Treatmeant, p.adjust.method = "bonferroni")

# Print pairwise comparison results
print(post_hoc_test)

timepoints <- unique(P13FI$Timepoint)
for (tp in timepoints) {
  # Subset data for the current timepoint
  subset_data <- subset(P13FI, Timepoint == tp)

  # Perform ANOVA for the subset data
  anova_result <- aov(Antenna_MeanI ~ Treatmeant, data = subset_data)

  # Apply Tukey HSD for post-hoc pairwise comparisons
  tukey_result <- TukeyHSD(anova_result, "Treatmeant")

  # Print the results for each timepoint
  cat("\nTimepoint:", tp, "\n")
  print(tukey_result)
}
```

## Code for fluorescent intensity comparisons at specific time points

```
##For all plates, DPI 8
DPI8_FI<- read.csv('Sodalis_PupaeInjections - DPI15_Egg_Clean.csv')
# Ensure categorical variables are factors
DPI8_FI$Treatmeant <- factor(DPI8_FI$Treatmeant)
DPI8_FI

custom_colors <- c(
```

```
  "2K" = "brown1",
  "1K" = "tan1",
  "PBS" = "yellowgreen"
)

ggplot(DPI8_FI, aes(x = as.factor(Treatmeant), y = Eggs, fill = Treatmeant)) +
  geom_boxplot(alpha = 0.5, outlier.shape = NA) +  # Boxplot without outlier dots (to avoid
duplication)
  geom_point(aes(color = Treatmeant),
             position = position_dodge(width = 0.75),  # Align points with boxplots
             alpha = 1, size = 1) +  # Adjust transparency & size
  labs(x = "Treatment", y = "Number of Eggs", title = "Number of eggs laid") +
  scale_fill_manual(values = custom_colors) +
  scale_color_manual(values = custom_colors) +  # Set y-axis range from 0 to 4000
  theme_minimal() +
  theme(
    axis.title = element_text(family = "Arial", size = 14),  # Axis labels font
    axis.text = element_text(family = "Arial", size = 14),  # Axis tick labels font
    legend.title = element_text(family = "Arial", size = 14),  # Legend title font
    legend.text = element_text(family = "Arial", size = 14)  # Legend labels font
  ) +
  geom_signif(comparisons = list(c("PBS", "1K"),
                                 c("1K", "2K"), c("PBS", "2K")),
              map_signif_level = TRUE,
              y_position = c(18, 18, 20))

table(DPI8_FI$Treatmeant)
anova_result_DPI8_I <- aov(MeanI ~ Treatmeant, data = DPI8_FI)
# Summary of the ANOVA results
summary(anova_result_DPI8_I)

# Extract residuals from the ANOVA model
residuals_DPI8_I <- residuals(anova_result_DPI8_I)

# Perform Shapiro-Wilk test for normality
shapiro_test <- shapiro.test(residuals_DPI8_I)
# Print the result
print(shapiro_test)
kruskal_test <- kruskal.test(MeanI ~ Treatmeant, data = DPI8_FI)
print(kruskal_test)
library(FSA)
dunn_test <- dunnTest(MeanI ~ Treatmeant, data = DPI8_FI, method = "bonferroni")
print(dunn_test)
```

```
# Tukey HSD post-hoc test for interaction
tukey_interaction_DPI8_I <- TukeyHSD(anova_result_DPI8_I, "Treatmeant")
# Print results
print(tukey_interaction_DPI8_I)
```

## Code for Motality Analysis

```
library(survival)
library(coxme)
library(survminer)
library(ggplot2)
library(dplyr)

setwd("/Users/ashmitabaruah/Desktop/MPI_CE/Stats/ABPVExp/Feb2025")
coxtable <- read.csv('SurvivalData_ABPV_URL - ABPVPilot1_coxformat.csv')

# Ensure categorical variables are factors
coxtable$Treatment <- factor(coxtable$Treatment)
coxtable$Type <- factor(coxtable$Type)
coxtable$Replicate <- as.factor(coxtable$Replicate)

# Correct Status coding (1 = censored, 0 = event/death)
coxtable$Status <- ifelse(coxtable$Status == 0, 1, 0)

# Create a new variable combining Treatment and Type
coxtable <- coxtable %>%
  mutate(Group = interaction(Treatment, Type, sep = "."))

# Ensure Group is a factor and explicitly set its levels
coxtable$Group <- factor(coxtable$Group, levels = unique(coxtable$Group))
coxtable

# Now safely relevel Group to set "Bee-extract.I" as baseline
coxtable$Group <- relevel(coxtable$Group, ref = "ABPV.I")

#Verification if the cox model can be used
coxph_model <- coxph(Surv(Timepoint, Status) ~ Group, data = coxtable)
test_ph <- cox.zph(coxph_model)
print(test_ph)
plot(test_ph)

# Fit Cox mixed-effects model using Group as predictor
coxme_model <- coxme(Surv(Timepoint, Status) ~ Group + (1 | Replicate), data = coxtable)
```

```
# View model summary
summary(coxme_model)

# Extract Hazard Ratios (HR) and 95% Confidence Intervals
ci_df <- data.frame(
  Variable = names(fixef(coxme_model)),
  HR = exp(fixef(coxme_model)),
  Lower = exp(fixef(coxme_model) - 1.96 * sqrt(diag(vcov(coxme_model)))),
  Upper = exp(fixef(coxme_model) + 1.96 * sqrt(diag(vcov(coxme_model))))
)

print(ci_df)  # Print Hazard Ratios

# Pairwise Log-Rank Test for all Groups with Benjamini-Hochberg adjustment
pairwise_results <- pairwise_survdiff(Surv(Timepoint, Status) ~ Group,
                                      data = coxtable,
                                      p.adjust.method = "BH")
print(pairwise_results)

# Kaplan-Meier Survival Plot for all Groups
km_fit <- survfit(Surv(Timepoint, Status) ~ Group, data = coxtable)

custom_colors <- c(
  "ABPV.I" = "brown1",
  "ABPV.CH" = "orchid",
  "Bee_extract.I" = "yellowgreen",
  "Bee_extract.CH" = "steelblue1"
)

km_plot <- ggsurvplot(
  km_fit,
  data = coxtable,
  conf.int = TRUE,  # Show confidence intervals
  xlab = "Timepoint (hrs post injection)",
  ylab = "Proportion of Individuals Alive",
  ggtheme = theme_minimal(),
  title = "Kaplan-Meier Survival Curves Across Groups",
  legend.title = "Group",
  legend.labs = levels(coxtable$Group),
  palette = custom_colors
)

# 🔹 Ensure x-axis is linear and shows exact Timepoint values
```

```
km_plot$plot <- km_plot$plot +
  scale_x_continuous(breaks = sort(unique(coxtable$Timepoint))) +  # Rotate labels for
readability
  theme(
    axis.title = element_text(family = "Arial", size = 11),  # Axis labels font
    axis.text = element_text(family = "Arial", size = 11),  # Axis tick labels font
    legend.title = element_text(family = "Arial", size = 11),  # Legend title font
    legend.text = element_text(family = "Arial", size = 11)  # Legend labels font
  )

# Print the updated Kapln-Meier Plot
print(km_plot)
```